Direct observation and reactivity of oxenium ions

by

Patrick James Hanway

A dissertation submitted to the graduate faculty

in partial fulfillment of the requirements for the degree of

DOCTOR OF PHILOSOPHY

Major: Organic Chemistry

Program of Study Committee
Arthur H. Winter, Major Professor
William Jenks
Theresa Windus
Keith Woo
Malika Jeffries EL

Iowa State University

Ames, Iowa

2014

TABLE OF CONTENTS

ACKNOWLEDGEMENTS

I would like to start by thanking my advisor Dr. Winter. For the last 5 years you have provided the knowledge, patience, and experience necessary to make me into a better chemist as well as person. You have been a great advisor and I wish you the best in the future. I would also like to thank my committee members: Dr. Theresa Windus, Dr. William Jenks, Dr. Malika Jeffries-El, and Dr. Keith Woo. Your support and guidance was greatly appreciated. I would also like to thank my friends in Ames: Adam, Andy, Gargey, and Ben. You made the transfer to graduate school significantly easier and more entertaining. I would like to thank my family, and in particular, my mother, for listening to my rambling about research as well as her endless support. Thanks to all my friends in Missouri who make time in their schedules whenever I have the ability to return home. Thanks to Sarah Cady for her endless magnetic knowledge. I would also like to thank the Winter lab group members for your help in personal and group goals. I wish you all well in your future careers. I would like to thank Andy and Gargey for helpful afternoon discussions. Thanks to Dr. Phillips and his post-doctoral students that have helped with studies on oxenium ions. The insight that we gained from the LFP and TR3 experiments added significantly to our research. Thanks to GP3 for sports conversations. Thanks also to Christicle for helpful research/career discussions. I'll miss your series of endless compliments, and the feeding frenzy and Mario party parties. You have been my best friend since our first year and I will miss you. A special thanks also to the person who made Ames my first real home away from home. To the numerous people not mentioned here that have added to my life here in Ames, I thank you. I wish you all the best.

ABSTRACT

Oxenium ions are poorly understood reactive intermediates of the formula R-O^+. This body of work is an accumulated computational and experimental investigation into understanding the electronic configuration, spectroscopic signatures, spin-selective reactivity, and lifetimes of these short-lived intermediates.

Chapter 1 overviews our attempts to find a photochemical precursor to oxenium ions, which ultimately led to the first direct detection of the short-lived parent phenyloxenium ion. Laser flash photolysis studies were performed on the phenyl hydroxylamine tetrafluoroborate salt to form the singlet phenyloxenium ion. These studies were performed by Jiadan Xue in the lab of Dr. David Lee Phillips. The lifetime for the phenyloxenium ion was found to be about 5 ns. Product studies from both thermolysis and photolysis with added traps suggest the formation of the phenyloxenium ion along with the phenoxy radical.

In order to better understand the effect of structure on the electronic configuration of oxenium ions, Chapter 2 provides an in depth study of heteroaryl oxenium ions by high-level multireference CASSCF/CASPT2 calculations. 4-pyridinyl, pyrizidinyl, and pyrimidyl oxenium ions all have singlet-triplet gaps (ΔE_{ST}) of less than -4 kcal/mol, showing significantly changed electronics from the parent phenyloxenium ion. This small gap suggests the possibility that triplet states as well as open shell singlet states could be chemically relevant to these intermediates.

In chapter 3, the synthesis of a photochemical precursor to the p-biphenylyl oxenium ion is described, and the ultrafast LFP experiments performed by Mingde Li in the lab of Dr. David Lee Phillips on this precursor suggest photolysis leads to the p-

biphenylyl radical, as well as the p-biphenylyl oxenium ion as a closed shell singlet, open shell singlet, and a triplet state.

Chapter 4 describes the synthesis of a photoprecursor to the m-dimethylamino phenyloxenium ion, which is computed to have a triplet ground state (+12 kcal/mol, B3LYP/cc-PVTZ). Photolysis of this precursor was studied using product studies as well as by matrix isolation EPR studies. The results obtained by matrix isolated EPR provide evidence that the ground state of the m-dimethylamino phenyloxenium ion is a ground state triplet.

CHAPTER 1
INTRODUCTION

Oxenium ions are hypovalent species of formula R-O^+. As isoelectronic species with nitrenes, these reactive intermediates contain a formally monovalent oxygen with two nonbonding pairs of electrons. The electron deficient nature of these intermediates makes them powerful electrophiles. This effect is increased due to placing a formal positive charge on an electronegative oxygen.

Reactive intermediate family. It is useful to compare the structure of oxenium ions to related hypovalent reactive intermediates such as carbenes, nitrenes, and nitrenium ions. These species are shown in Figure 1.

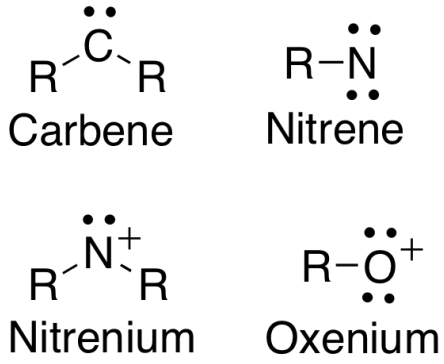

Figure 1: Family of reactive intermediate species.

Oxenium ions are isoelectronic species with nitrenes, being monovalent species with two lone pairs, but a difference is that oxenium ions are charged rather than neutral. Similarly, nitrenium ions are charged but have an extra bond as opposed to a non-bonding pair of electrons. Since these species are similar, much information can be gained by understanding what is known of these related species. To date, a significant amount of work has been done on these related species.[1-5]

Oxenium ions as intermediates in industrially-important reactions.

Oxenium ions are increasingly being proposed as intermediates for a number of reactions. For example, they are proposed intermediates in numerous phenol and alkane oxidations,[6-8] particularly those catalyzed by hypervalent iodine and copper catalysts. A few of these are shown in Figure 2.

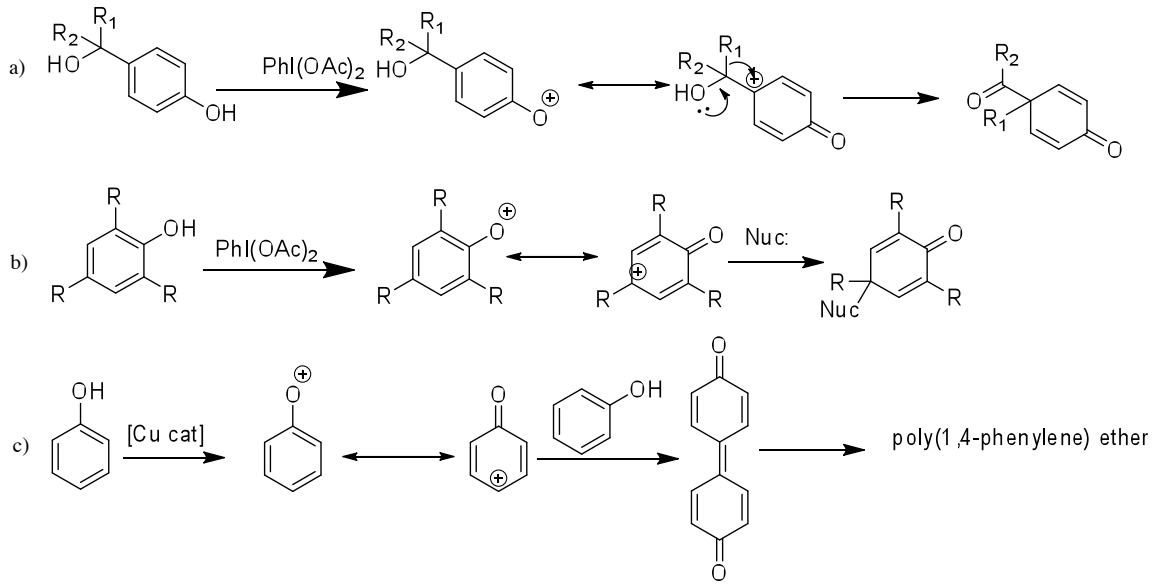

Figure 2: Proposed synthetic schemes involving aryloxenium ion intermediates.

Both a and b of Figure 2 show a phenolic group going through an oxenium ion in order to form more substituted quinone structures. In Figure 2c phenol is converted to poly(1,4-phenylene) ether (PPE), a high-value industrial thermoplastic. Phenol, which is produced on a 7-billion kg/year scale,[9] is converted into this high value thermoplastic, which can also be blended with other materials such as polystyrene in order to produce high quality products.[10,11] An example of this is the use of PPE's as flame retardant materials.[12] In order to better optimize and understand reactions involving these intermediates, more fundamental research into these intermediates is needed.

Electronic configurations dictate reactivity

One thing that is known of these related species is the importance of the electronic state on the reactivity of the reactive intermediate. At least in principle, a number of different electronic configurations can be envisioned for hypovalent species containing two electrons to be placed into two empty orbitals. These include closed shell singlets (Figure 3a) triplet states (Figure 3c), or open-shell singlets (Figure 3b).

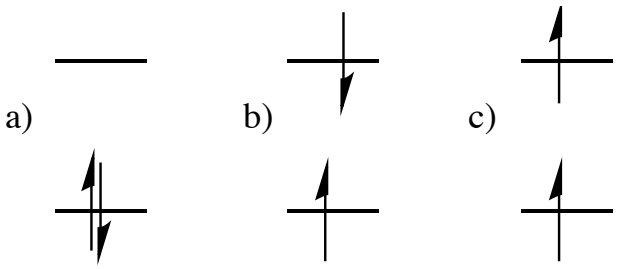

Figure 3. Electronic configuration of a closed shell singlet state.

It is important to understand the electronic configuration adopted by a reactive intermediate because the electronic configuration a molecule adopts will dictate the reactivity of the molecule. An example of this spin-selective reactivity for carbenes is shown in Figure 4.

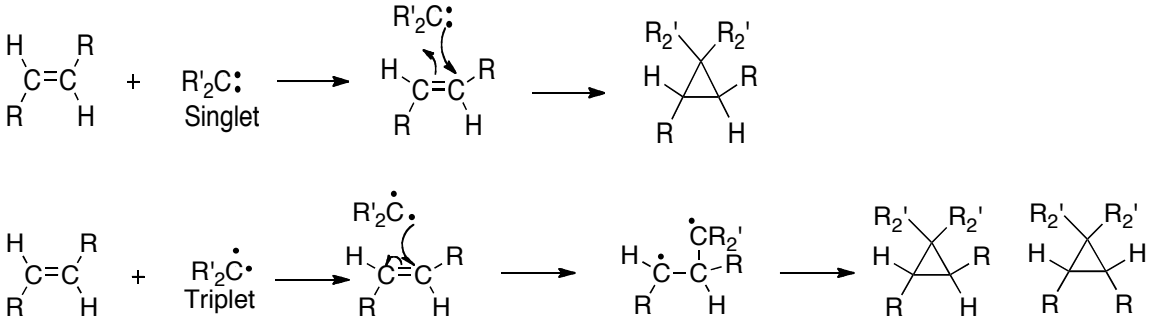

Figure 4. Spin selective reactivity of singlet vs. triplet carbenes.

As can be seen, a singlet carbene acts as a typical two-electron nucleophile and adds in a concerted fashion to alkenes. In the case of the triplet carbene, the alkene

reaction is stepwise involving the intermediacy of a diradical, allowing for bond rotation and leading to a mixture of stereoisomers.

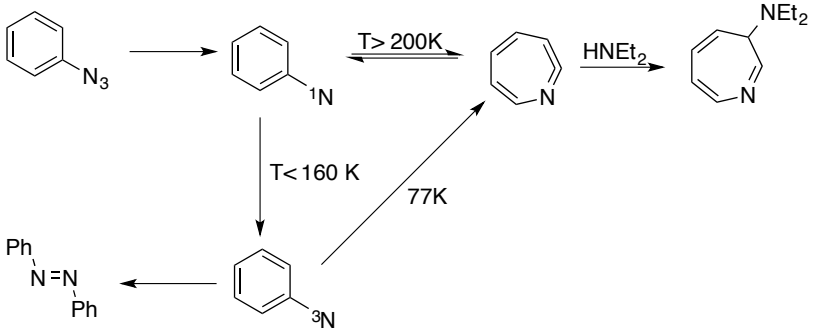

Figure 5. Reaction scheme of phenylnitrene through temperature based singlet vs triplet chemistry.

Figure 5 shows how temperature can dictate the reactivity of phenylnitrene. As can be see, if the nitrene reacts as a singlet versus a triplet, very different products are obtained. This selectivity of pathways shows the power of the electronic configuration in product formation. In the case of the singlet state, a ring expansion and trapping occurs, while the triplet state undergoes a dimerization to make an azobenzene product.

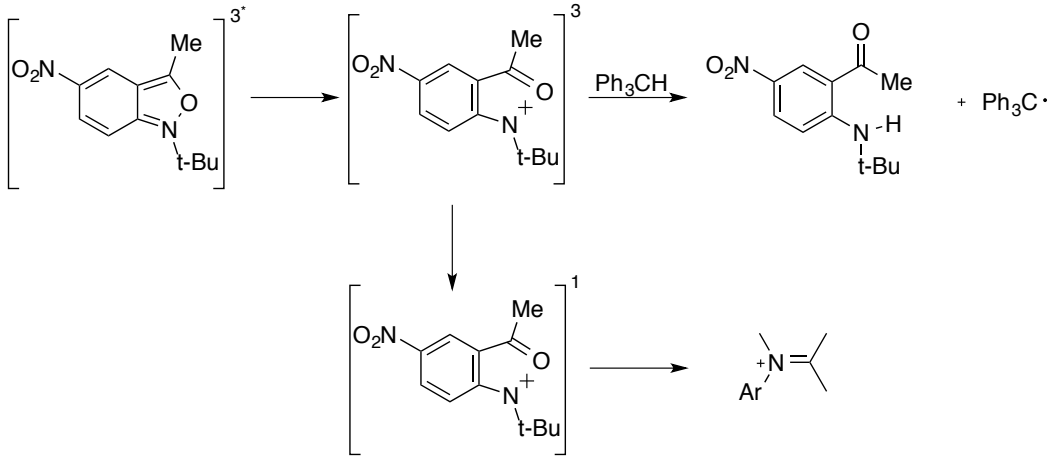

Figure 6. Arylnitrenium ion through triplet chemistry (top) and singlet chemistry (bottom).

Nitrenium ions also show spin-selective reactivity. The example in Figure 6 shows an arylnitrenium ion, which through the triplet state forms the parent amine via an H-atom abstraction process. Through singlet chemistry, however, it forms the iminium ion. Even though most phenylnitrenium species are ground state singlets, some can still go through triplet chemistry and even be ground state triplets.

It is important to keep in mind that the observation of typical singlet or triplet reactivity is not necessarily proof that it is the ground state. As is the case with some ground state triplet nitrenes that decay through singlet paths since the reactions of the singlet nitrene occurs quicker than that of intersystem crossing.

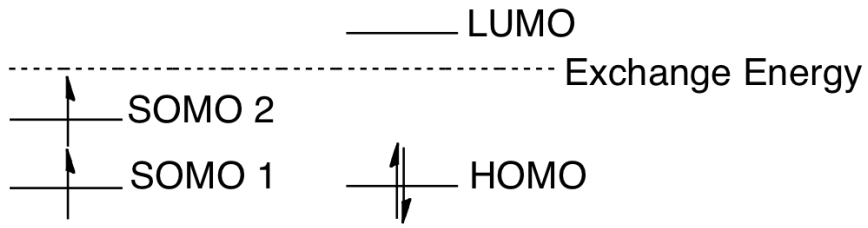

Figure 7. Orbital representation of singlet (right) and triplet (left) ground states.

It is important to understand the factors that influence whether a reactive intermediate will be open-shell singlet, closed-shell singlet, or triplet. A simplistic analysis focuses on the frontier orbitals and the exchange energy of the two electrons being placed into the two orbitals. If the energy gap between the two orbitals is smaller than the exchange energy of the molecule, then it will be a ground state triplet (Figure 7). However, if the energy gap is greater than that of the exchange energy then the intermediate will be a ground state singlet (Figure 7). Thus, in general, reactive intermediates with small frontier orbital gaps (or degenerate frontier orbitals) usually have triplet ground states, while reactive intermediates with large gaps tend to have singlet ground states.

Electronic configuration of oxenium ions.

The parent oxenium ion, the hydroxy cation ^{+}OH, is a ground-state triplet ion ($^{3}\Sigma^{-}$) with a large adiabatic energy gap of 54 kcal/mol to the lowest-energy singlet state ($^{1}\Delta$).[13] This lower energy triplet state in this ion results from a degeneracy in the *p* orbitals, as illustrated in Figure 8, leading to adoption of a lowest energy unpaired spin state following a molecular orbital extension of Hund's rule. The lowest energy singlet state is an open-shell singlet.

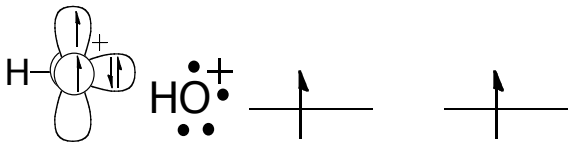

Figure 8. Electronic configuration for the hydroxy cation.

Currently structural effects on oxenium ion electronic configurations are not well known. Experimental work thus far on aryloxenium ions implicate closed shell singlet chemistry as opposed to diradical chemistry.[14-20] Computational work also suggests that the ground state of most aryloxenium ions will be the ground state closed shell singlet.[21]

Aryloxenium ions have been generated through photochemical or thermochemical methods in past studies. Abramovich and Okamoto performed thermolysis reactions to generate aryloxenium ions, and product studies were used to characterize the intermediates due to the absence of direct characterization methods.[14-16,22,23] Since then the lab of Novak has also studied the reactivity of aryloxenium ions through indirect means as well.[18] In 2007 the labs of Novak and Platz provided the first direct detection of an aryloxenium ion by the use of laser flash photolysis and found the lifetime to be 170 ns in water.[24]

Laser Flash Photolysis allows for direct detection of oxenium ions.

In the experimental arena, the biggest advancement in the field of reactive intermediates has been the addition of laser flash photolysis. This allows for the direct observation of these short-lived intermediates in the nano- or pico-second time frame. Laser flash photolysis is a system where a laser pulse is generated and this pulse travels to the sample and excites the sample. The intermediate is formed and the detector observes the decay of the intermediate(s). A simplistic view of a general LFP system is shown in Figure 9.

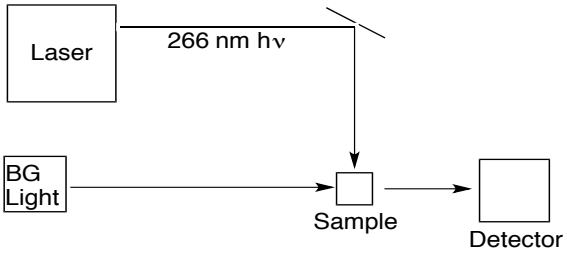

Figure 9. General setup for a laser flash photolysis experiment.

The absorbance of the initial starting material is the background spectrum for the experiment. This is subtracted from all of the following spectra so if the starting material shows up in the wavelengths that are observed, then it will be shown as a negative peak. The intermediate(s) will be at their max initially after excitation and will decay over time as shown in Figure 10. A system that has multiple intermediates could have one intermediate decay into a new peak that would be the second intermediate of the reaction. This allows for the observation of the second intermediate as well.

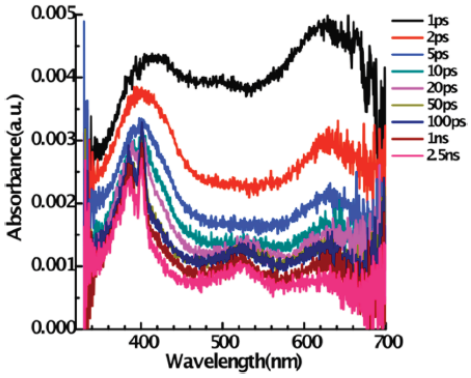

Figure 10. LFP of a sample molecule's intermediate decay.

The max intermediate wavelength can be monitored and a spectrum as shown in Figure 11 can be obtained. This spectrum allows for the lifetime of the intermediate species to be obtained.

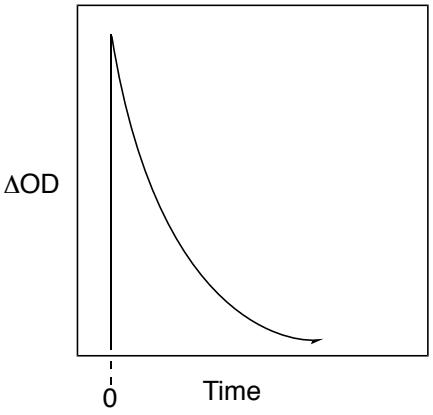

Figure 11. Single wavelength decay of an intermediate peak.

A series of these single wavelength decays can also be coupled together in experiments with trapping solvents to allow for trapping rate constants to be obtained. Comparing these spectra to computational UV-vis spectra can also help in the assignment of peaks.

Complete active space self consistent field (CASSCF) calculations for insight into oxenium ions.

Computational analysis can be extremely helpful in investigating the electronic configurations of reactive intermediates. Typically, single-reference computations (such as density functional theory) give good estimates for singlet-triplet gaps. However, when calculating singlet triplet gaps of reactive intermediates that are not well described by a single-reference wavefunction, more sophisticated methods must be used. Most standard calculations are single-reference: that is, they only consider one configuration in the calculation. Take for example Figure 12.

Figure 12. Typical electron configuration used for single reference calculations.

The entire calculation will be done on this electronic structure with an occupation of each orbital being 0 or 2. However, as is sometimes the case with reactive intermediate structures this can give poor results if the ground-state wavefunction is described by a combination of multiple configurations.

One approach to including these multiple configurations is to use complete active space self-consistent field (CASSCF) calculations. An active space is selected (represented by brackets in Figure 13), and in that active space the electrons are allowed to take on different configurations. The total wave function then becomes a combination of all the different active space wave functions as shown below.

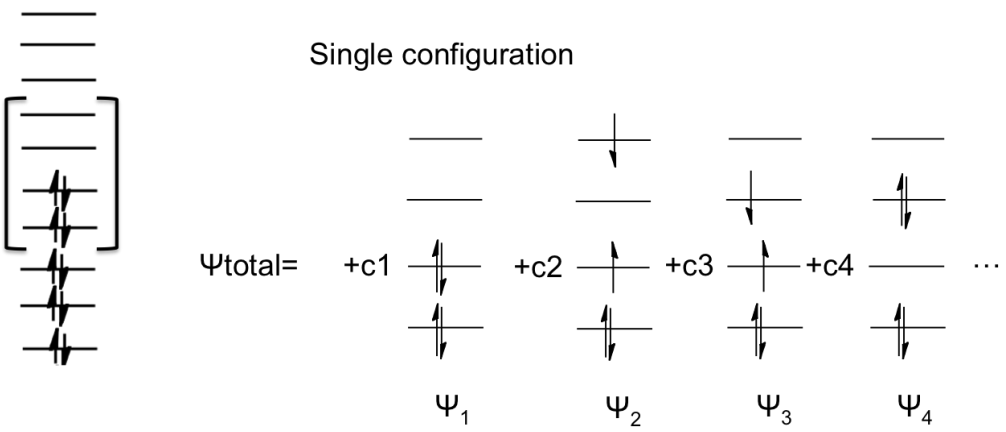

Figure 13. An example of a CASSCF total electronic configuration as a mixture of active space configurations.

Outside of the active space the computation uses the normal occupation states of 0 or 2. This makes the choice of active space very important. If important orbitals or electrons are not included then the results will suffer. The lower and upper orbitals don't need to be included as long as they are well represented with an orbital occupation of 2 or 0. When accurate energies are required, this method can be modified by using CASPT2, which accounts for electron correlation outside of the active space using second-order perturbation theory.

Aryloxenium ions. While the hydroxy cation has degenerate frontier orbitals, and is thus a ground-state triplet ion, for aryloxenium ions the electronic configuration is less clear. Since the aryl ring interacts differently with the two p orbitals this breaks the degeneracy of the two p orbitals. The question then becomes: will the orbital energy difference be large, leading to a HOMO-LUMO gap that is greater than the exchange energy (Figure 14) leading to a ground state singlet? Or will the exchange energy be lower than the energy gap, leading to a ground state triplet? This idea is illustrated in Figure 14.

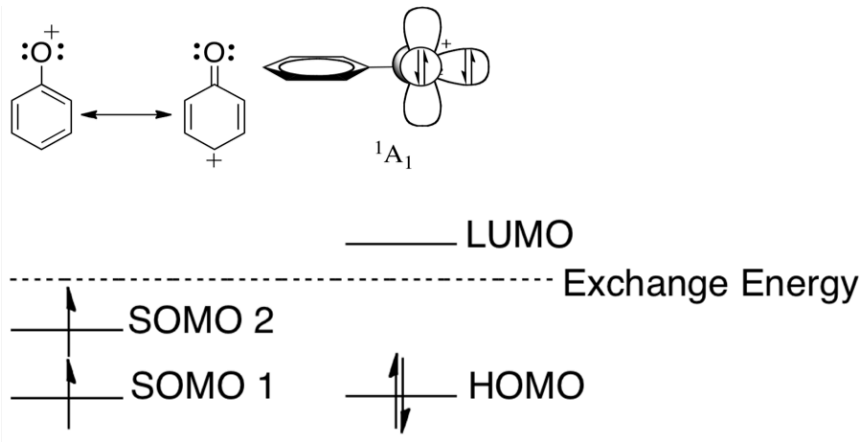

Figure 14. Image of exchange energy vs orbital energy gap potentially leading to the ground state singlet or triplet.

Recent Work on Aryloxenium ions.

A recently published paper provided computational insight into what to expect with the phenyloxenium ion and related ions.[21] This paper computed the phenyloxenium ion to have a ground state closed shell singlet ($^1A_1$) that was -22 kcal/mol lower in energy than the nearest triplet state ($^3A_2$).[21] This correlated very well with the experimental study that showed a gap of -19.8 kcal/mol.[25] These computations were done using high-level multireference CASSCF/CASPT2 computations. These calculations were used due to their high level of accuracy with related species such as nitrenium ions. This drastic swing from the parent hydroxy cation comes from the loss of the degeneracy of the p orbitals due to the π system mixing with the p orbital. As the degree of mixing in the two orbitals increase, a larger HOMO-LUMO gap results and leads to a ground state singlet configuration.

In this study different substitutions were calculated in order to see how simple changes on the phenyloxenium ion would affect singlet/triplet energies.

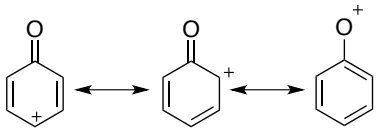

Fig 15. Resonance structures of the closed-shell singlet phenyloxenium ion.

Since the phenyloxenium ion has resonance structures that place the positive charge on the ortho and para position (Figure 15), it would be expected for those positions to have an effect on the electronics. This was indeed the case, as is shown in Figure 17.

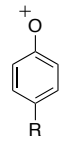

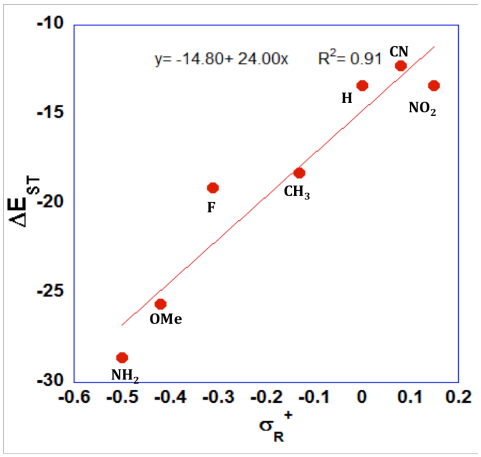

Figure 16. Effect of para substituents on the phenyloxenium ion.

As can be seen in Figure 16, electron-donating groups such as NH_2 led to a larger singlet triplet gap whereas electron-withdrawing groups led to a smaller singlet triplet gap. This occurs because electron-donating groups raise the energy of the π orbital closer to that of the oxygen p orbital, thus increasing the mixing of the orbitals. This increased mixing leads to a stabilization of the ground state singlet. Unlike the ortho and para position however, there is no resonance form of the phenyloxenium ion that places the positive charge on the meta position. This lack of resonance makes it less intuitive as to how

meta substituents would influence the singlet-triplet gap. Figure 17 provides the computed results obtained for meta substituents. Electron withdrawing groups and groups that are not strong donors/withdrawers at the meta position have very little effect on the singlet triplet gap. Highly electron-donating groups, on the other hand, have a drastic relative stabilization of the triplet state. This drastic change was found to be primarily due to the destabilization of the singlet state, and it has only minor differences on the triplet state energy.

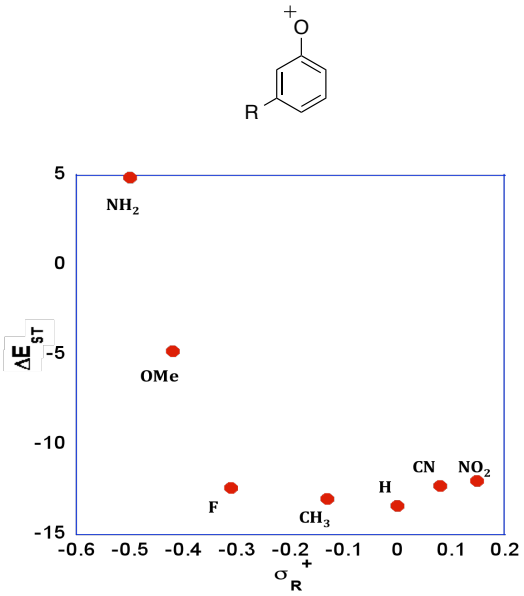

Fig 17. Effect of meta groups on the ΔE_{ST} of the phenyloxenium ion.

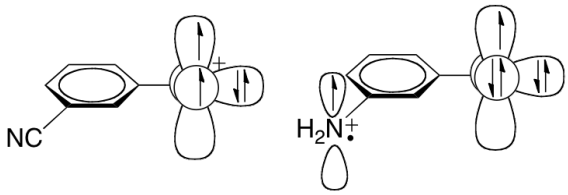

Figure 18. Lowest energy triplet configuration for meta amino- and meta cyano-phenyloxenium ions.

This drastic change was also found to occur along with the switch from an n to π* triplet state to a π to π* triplet state (Figure 18).

The major potential advantage of this knowledge is that now there seems to be a very easy and direct way to create a molecule that would have a ground state triplet oxenium ion, which to date has not been directly observed and could provide for some interesting chemistry.

REFERENCES

(1) Zhang, Y.; Burdzinski, G.; Kubicki, J.; Platz, M. S. *J. Am. Chem. Soc.* **2008**, *130*, 16134.

(2) Wang, J.; Burdzinski, G.; Kubicki, J.; Platz, M. S. *J. Am. Chem. Soc.* **2008**, *130*, 11195.

(3) Platz, M. S. *Acc. Chem. Res.* **1995**, *28*, 487.

(4) Winter, A. H.; Thomas, S. I.; Kung, A. C.; Falvey, D. E. *Organic Letters* **2004**, *6*, 4671.

(5) Winter, A. H.; Gibson, H. H.; Falvey, D. E. *J. Org. Chem.* **2007**, *72*, 8186.

(6) Olah, G. A., Molnar, A. *Hydrocarbon Chemistry*; John Wiley & Sons: Hoboken, NJ, 2003.

(7) Peng, H. M.; Webster, R. D. *J. Org. Chem.* **2008**, *73*, 2169.

(8) Williams, L. L.; Webster, R. D. *J. Am. Chem. Soc.* **2004**, *126*, 12441.

(9) *J. Am. Chem. Soc.* **2003**, *125*, 10768.

(10) Ishii, Y.; Ryan, A. J. *Macromolecules* **1999**, *33*, 167.

(11) *Applications of Anionic Polymerization Research*; American Chemical Society, 1998; Vol. 696.

(12) Granzow, A. H.; Google Patents: 1981.

(13) Katsumata, S.; Lloyd, D. R. *Chemical Physics Letters* **1977**, *45*, 519.

(14) Abramovitch, R. A.; Inbasekaran, M.; Kato, S. *J. Am. Chem. Soc.* **1973**, *95*, 5428.

(15) Abramovitch, R. A.; Alvernhe, G.; Inbasekaran, M. N. *Tetrahedron Lett.* **1977**, 1113.

(16) Abramovitch, R. A.; Alvernhe, G.; Bartnik, R.; Dassanayake, N. L.; Inbasekaran, M. N.; Kato, S. *J. Am. Chem. Soc.* **1981**, *103*, 4558.

(17) Novak, M.; Poturalski, M. J.; Johnson, W. L.; Jones, M. P.; Wang, Y. T.; Glover, S. A. *J. Org. Chem.* **2006**, *71*, 3778.

(18) Novak, M.; Glover, S. A. *J. Am. Chem. Soc.* **2004**, *126*, 7748.

(19) Novak, M.; Glover, S. A. *J. Am. Chem. Soc.* **2005**, *127*, 8090.

(20) Sabot, C.; Commare, B.; Duceppe, M. A.; Nahi, S.; Guerard, K. C.; Canesi, S. *Synlett* **2008**, 3226.

(21) Hanway, P. J.; Winter, A. H. *J. Am. Chem. Soc.* **2011**, *133*, 5086.

(22) Shudo, K.; Orihara, Y.; Ohta, T.; Okamoto, T. *J. Am. Chem. Soc.* **1981**, *103*, 943.

(23) Endo, Y.; Shudo, K.; Okamoto, T. *J. Am. Chem. Soc.* **1982**, *104*, 6393.

(24) Wang, Y. T.; Jin, K. J.; Leopold, S. H.; Wang, J.; Peng, H. L.; Platz, M. S.; Xue, J. D.; Phillips, D. L.; Glover, S. A.; Novak, M. *J. Am. Chem. Soc.* **2008**, *130*, 16021.

(25) Dewar, M. J. S.; David, D. E. *J. Am. Chem. Soc.* **1980**, *102*, 7387.

CHAPTER 2:
DIRECT DETECTION AND REACTIVITY OF THE SHORT-LIVED PHENYLOXENIUM ION

Taken in part from:
Hanway, P. J.; Xue, J.; Bhattacharjee, U.; Milot, M. J.; Ruixue, Z.; Phillips, D. L.; Winter, A. H. *J. Am. Chem. Soc.* **2013**, *135*, 9078.

INTRODUCTION

A major roadblock that has stymied the detailed study of oxenium ions is the lack of suitable photoprecursors to these ions. Studies of related intermediates such as carbenes,[1,2] nitrenes,[3−5] and nitrenium ions[6−8] have benefited tremendously from the ability to generate these species photochemically from established precursors (e.g., aryl azides, diazo compounds, etc.), permitting detailed spectroscopic studies of their reactivity and properties. In contrast, there are few photoprecursors to oxenium ions. Some reports suggest oxenium ions can be formed as part of intermediate mixtures from multiphoton ionization studies or from mass spectral ion fragmentations,[9-12] but recent attempts at developing robust single-photon precursors to these species suitable for mechanistic studies, by either photolysis or thermolysis, have proven to be challenging.[13−16] However, in exciting recent studies reported by Novak and Platz, a 4′-methyl-4-biphenylyloxenium ion was generated by photolysis of the 4-(4-methylphenyl)-4-acetoxy cyclohexadienonyl derivative (shown in Scheme 1).[14,17] These studies were significant because they demonstrated the direct observation of a discrete oxenium ion using laser photolysis. This photoprecursor has the limitation that it requires a **para** substituent to prevent tautomerization, making it unsuitable for the photogeneration of the parent phenyloxenium ion. However, it is of considerable interest to understand the reactivity of the phenyloxenium ion, since this species is the parent aryloxenium ion and

may allow benchmarking the reactivity of this class of reactive intermediate in comparison to the related phenylnitrene, phenylnitrenium ion, and phenylcarbene.

Scheme 1. Previous Example of LFP of the 4′-Methyl-4-biphenylyloxenium Ion[18]

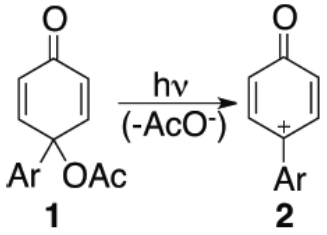

Thus, to generate the phenyloxenium ion, we required a new photoprecursor. On the basis of a report of **N** arylhydrazinium ions generating arylnitrenium ions upon photolysis,[19] we considered that **3** might similarly generate the phenyloxenium ion by photolysis, leading to O−N heterolytic scission with ejection of neutral ammonia. A potential advantage of this precursor (Scheme 2) is that it is positively charged rather than neutral, so that in principle the oxenium ion could be generated in any solvent system and would not be restricted to the ionizing solvents necessary for efficient generation of ion pairs from neutral precursors.

Scheme 2. Proposed Precursor for the Observation of the Phenyloxenium Ion **4**

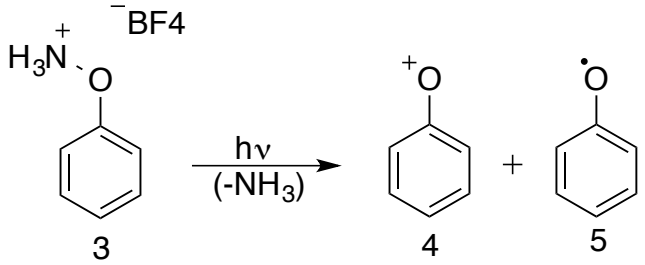

On the basis of laser flash photolysis studies ranging from the femtosecond to the microsecond time scale, product analysis, trapping experiments, and computed spectroscopic signatures, we find that photolysis of the protonated phenyl hydroxylamine

3 generates a short-lived intermediate consistent with the phenyloxenium ion as well as a longer-lived phenoxy radical.

The putative phenyloxenium ion is too short-lived to be significantly trapped by external nucleophiles other than solvent. The major products from photolysis and thermolysis of this precursor are phenol as well as the rearranged protonated **o**-/**p**-aminophenol and water adducts (hydroquinone, catechol), with photolysis leading to **para** adducts as the major products and thermolysis leading to an increased preference for **ortho** adducts.

RESULTS AND DISCUSSION

Laser Flash Photolysis (LFP) of **3**. Photolysis of 3 by LFP was performed in acetonitrile and a mixture of acetonitrile and water (9/1 and 1/1), using 266 nm excitation. The LFP spectra can be seen in Figure 1. A very broad, short-lived transient is observed immediately after the pulse ($\tau \approx 5$ ps), which we attribute to the excited state of **3**. Two longer-lived transients are also observed at later times after the excitation pulse. The first, having a set of absorptions at ~400 nm and a weaker band at 620 nm, can be assigned to the known spectrum of the phenoxy radical ($\tau = 150$ ns).[20−22] The slight blue shift and sharpening of the bands over ~30 ps is characteristic of vibrational cooling, wherein the vibrationally hot radical sheds heat to solvent. The lifetime of this 400 nm transient is not measurably reduced by an added azide trap, as would be expected of a radical and not a cationic species. The other transient is a broad absorption centered around 525 nm (after vibrational cooling) that is short-lived ($\tau = 3-20$ ns). We must provide a range for the lifetime of this transient, since the decay falls within the temporal "blind spot" between our femtosecond and nanosecond LFP setups the decay is too slow

to get a proper fit employing our femtosecond system, but the transient is gone within the detection limit (~20 ns) of our nanosecond setup. Unfortunately, having this transient decay within our temporal blind spot makes kinetic studies of this band difficult. However, on the basis of evidence described below, we assign this band to the phenyloxenium ion. Thus, the likely lifetime of this species is ~5 ns, with an upper limit on the lifetime of 20 ns, which is the shortest time we can observe with our nanosecond LFP setup.

Figure 1. LFP spectra of the precursor **3** in acetonitrile.

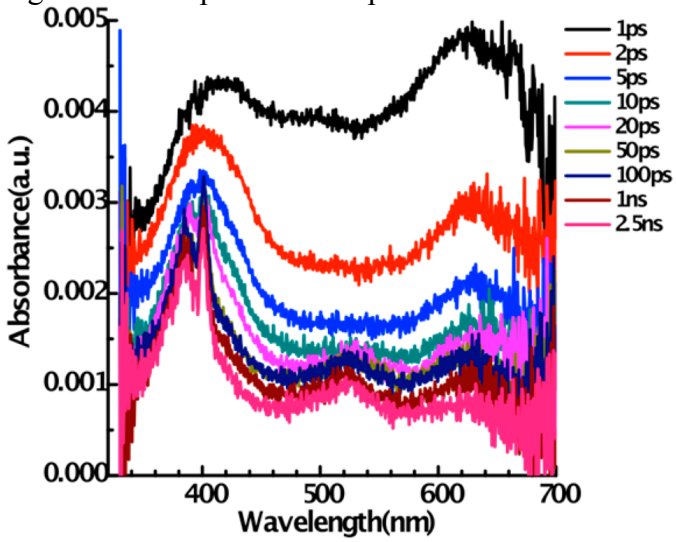

As further confirmation that the 400 nm transient is the phenoxy radical, we performed LFP experiments with time resolved resonance Raman (TR3) detection. The TR3 experiments using an incident beam at 400 nm (Figure 2) show a strong peak at 1490 cm−1, which correlates to reported values for the phenoxy radical.[21,23] Unfortunately, TR3 experiments with an incident beam at 532 nm to observe the resonance Raman spectrum of the putative oxenium ion gave no measurable spectrum. Possibly, the extinction coefficients and amounts of the presumed oxenium ion are too low to obtain a measurable spectrum using our experimental setup.

Figure 2. ps-KTR3 spectra at 12 and 100 ps of the precursor 3 along with computed spectra of the phenyloxenium ion (bottom) and the phenoxy radical (top). Asterisks represent solvent subtraction artifacts.

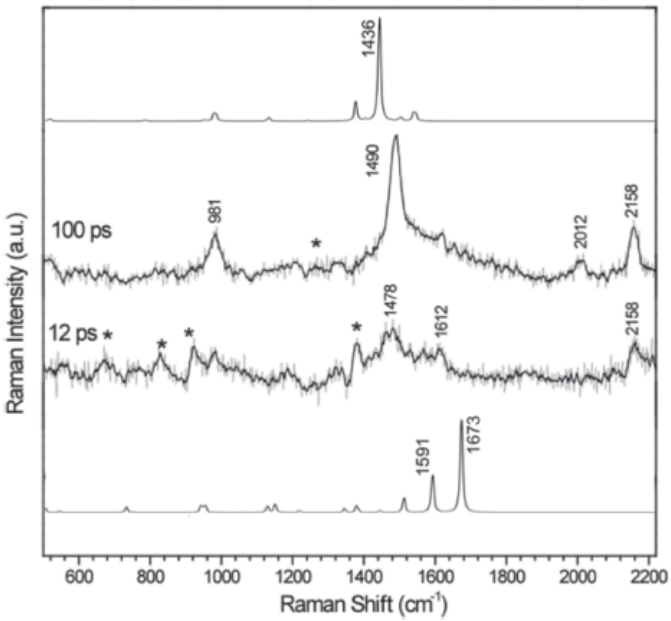

Assignment of the 525 nm Transient to the Phenyloxenium Ion.

While we were unable to obtain a TR3 spectrum of the 525 nm transient, a number of pieces of evidence suggest that it is the phenyloxenium ion. First, the laser flash photolysis spectra that we obtain are very similar to those seen for the previously reported 4′-methyl-4-biphenylyloxenium ion.[18] Photolysis of the acetyl precursor **1** led to two transients: a long-lived transient at lower wavelength (360 nm) corresponding to a biphenyloxy radical and a shorter-lived transient (170 ns, 460 nm) at higher wavelength corresponding to the 4′-methyl-4-biphenylyloxenium ion.[17,18] Our LFP studies give very similar results, with a long-lived band at ~400 nm (τ = 150 ns) that we can definitively assign to the phenoxy radical and a short-lived weakly absorbing band at 525 nm (τ = 3−20 ns).

Thus, the 525 nm transient absorption is in a location similar to that for the 4′-methyl-4-biphenylyloxenium ion, but with a shorter lifetime (τ = 120 ns for the 4′-

methyl-4-biphenylyloxenium ion in water), which would be expected of a less stabilized species. Second, previous studies have shown that TD-DFT can sometimes provide reasonable estimates of UV−vis spectra for related reactive intermediates.[24−26] Thus, we computed the absorption spectrum of the singlet phenyloxenium ion using TD-B3LYP/6-311+G(2d,p), shown in Figure 3.

Figure 3. Computed UV spectra (TD-B3LYP/6-311+G(2d,p)) of the phenyloxenium ion (red) and the phenoxy radical (blue).

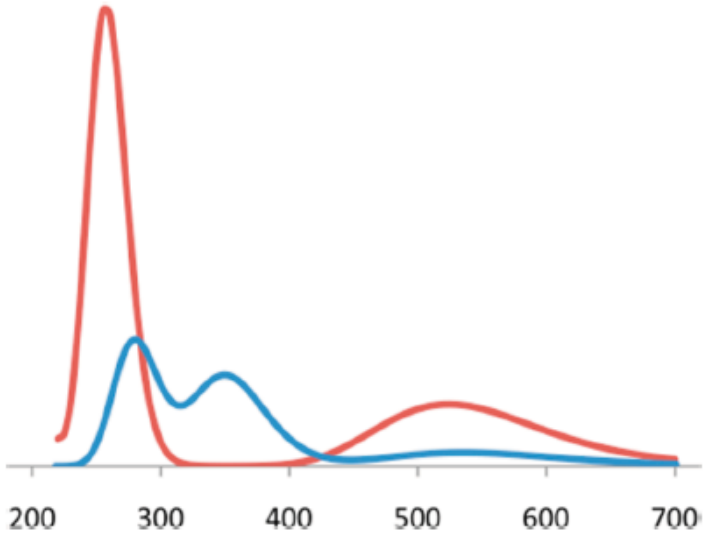

The computed absorption band for ^{1}**4** gives a single band in the visible region of the UV−vis spectrum centered at 524 nm, in good agreement with the experimental band (see Figure 1). Third, this 525 nm absorption is quenched as the solvent is changed to mixtures with increasing amounts of water (Figure 4). The band is largest in neat acetonitrile, smaller in 1/1 CH_3CN/H_2O, and negligible in 1/9 CH_3CN/H_2O.

Figure 4. LFP spectra of precursor 3 in different solvents obtained at ~500 ps.

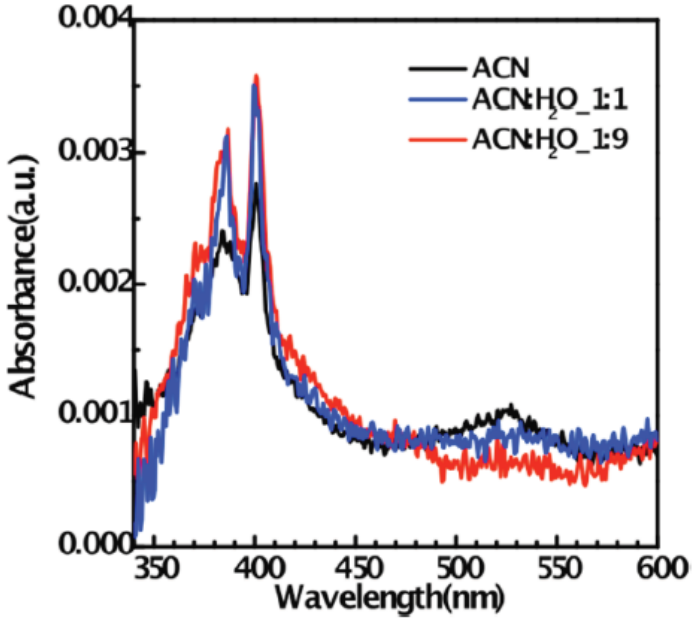

An example LFP spectrum is shown in Figure 5, which shows the LFP of precursor **3** in a 1:1 mixture of acetonitrile and water, and shows very little evidence of the peak near 525 nm as seen in Figure 1.

Figure 5: LFP of precursor **3** in ACN:H_2O 1:1

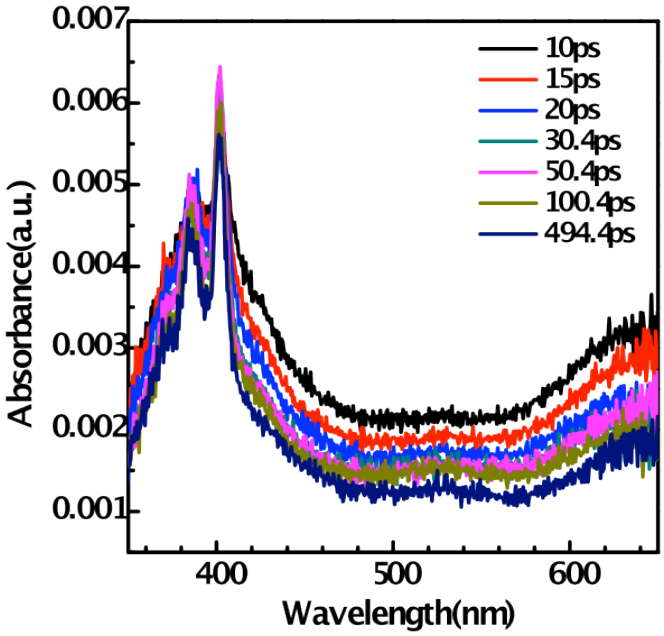

This quenching behavior by nucleophilic water would be expected of a highly electrophilic intermediate. Fourth, product studies from photolysis (and thermolysis) of **3** (described below) show small amounts of water adducts that would be expected of a cationic but not a radical intermediate. Finally, alternative assignments including a triplet excited state of **3** or the triplet oxenium ion ^{3}**4** seem less likely. Our DFT computations of the triplet excited state of **3** indicate that it is a dissociative state, optimizing to ammonia and the triplet phenyl oxenium ion ^{3}4. Further, our previous computational study indicates that **4** has a closed-shell singlet ground state, which is ca. 20 kcal/mol lower in energy than the lowest energy triplet state, making it less likely to be the triplet phenyloxenium ion.[1] Finally, the triplet oxenium ion ^{3}**4** is computed by TD-DFT to have major absorptions at 346 and 789 nm, in poor agreement with what we observe. Although in the absence of a TR3 spectrum it is hard to be definitive, the sum of this evidence leads us to assign this 525 nm band to the singlet phenyloxenium ion.

Photochemical and Thermal Product Studies of 3.

Products of the singlet oxenium ion are anticipated to derive from standard two-electron nucleophilic addition chemistry rather than diradical-type chemistry that is often associated with atom-centered triplets, such as the isoelectronic ground-state triplet phenylnitrene. Product studies were performed in different solvent systems, shown in Scheme 3. When the precursor is photolyzed in solvents containing water, the products are a mixture of protonated **o**- and **p**-aminophenol as well as the water adduct hydroquinone. We also see the 1/1/1 triplet at 6 ppm characteristic of the 1H NMR of the ammonium cation. **Ortho** and **para** ring adducts are characteristic of oxenium ions.[13,15,27–31]

Scheme 3. Product Studies on the Phenylhydroxylamine Tetrafluoroborate Salt **3**a. Yields were determined by ^{1}H NMR integration.

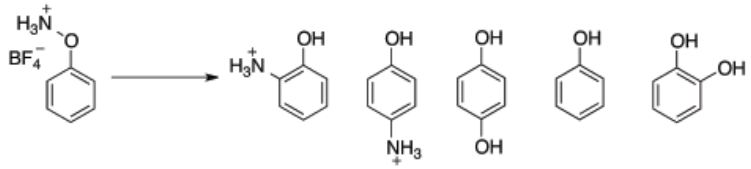

hν H_2O	52%	44%	4%	--	--
hν CH_3CN	38%	29%	--	33%	--
hν MeOH	40%	20%	--	40%	--
hν CH_3CN/H_2O 1:1	53%	42%	5%	--	--
hν MeOH/H_2O 1:1	53%	45%	2%	--	--
Δ, H_2O	50%	18%	18%	--	14%

The rearranged products could derive either from recombination of the phenoxy radical and ammonia radical cation or from recombination of ammonia with the phenyloxenium ion. The water adduct, hydroquinone, likely derives from water addition to the phenyloxenium ion. Phenol is also obtained in solvents other than water (e.g., neat MeOH, CH_3CN). Phenol may derive from either the phenoxy radical via a hydrogen atom abstraction process or from the phenyloxenium ion from a hydride transfer process. Addition of chloride as a trap, either in the form of added NaCl to solutions of **3** or from photolysis of the chloride salt of **3** rather than the BF_4^- salt, leads to only trace amounts of the **o**-/**p**-chlorophenol as detected by GC-MS.

It is possible that ejected ammonia may not undergo cage escape prior to recombination. This result suggests that the phenyloxenium ion is too short-lived to be trapped to a significant extent by externally added nucleophiles other than solvent under these conditions. The thermolysis of **3** in water gives products similar to those seen from photolysis. The major difference is that the thermolysis products show an increasing

preference for forming the **ortho** adducts in comparison to what is found under the photolysis conditions. Thus, larger amounts of **ortho** ammonium phenol are formed as well as catechol along with hydroquinone. The mechanism for the products are outlined in Figure 6. One possibility for this increasing preference for formation of the **ortho** adducts could be that the thermolysis conditions are under thermodynamic control. We performed DFT computations of the Wheland σ complex for addition of water and ammonia to the **ortho** and **para** positions. For both the protonated aminophenol and the dihydroxybenzene cases, the **ortho** σ complex was found to be lower in energy than the **para** σ complex. These lower energies could be attributed to the **ortho** σ complexes having access to an internal hydrogen bond (in the case of water addition to the ortho position of the phenyloxenium ion, geometry optimization leads to a proton transfer from the water to the aryl oxygen apparently without a barrier). The transition states were also computed for return of the **ortho** and **para** Wheland intermediates to the water-bound oxenium ion. Barriers for this back-reaction were found to be reasonably small (11 and 7 kcal/mol, respectively). However, it is also important to consider that a low-barrier tautomerization of the Wheland intermediate to the final aromatic product may effectively render the reaction irreversible. An alternative explanation is that the thermolysis leads to a larger partitioning toward the oxenium ion rather than the radical, leading to more solvent adducts and the differing product ratios. Our preliminary product studies of a protonated hydroxylamine precursor to the biphenylyl oxenium ion are suggestive that this latter explanation is more likely to be the correct one.

Figure 6: Potential mechanistic pathways that lead to the formation of the photolysis products.

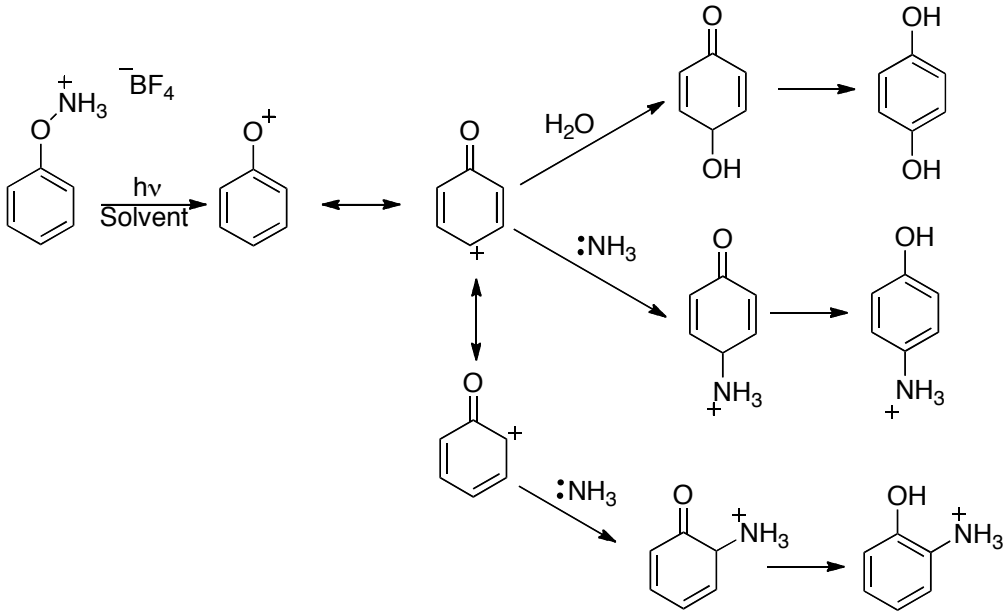

CONCLUSIONS

Photolysis of phenylhydroxylamine salt **3** leads to the phenoxy radical as well as a short-lived transient we assign to the phenyloxenium ion. This photoprecursor has a number of advantages, including a simple synthesis and the theoretical possibility to generate other oxenium ions in nonionizing solvents. A derivative of this precursor that cleanly generates oxenium ions in a general way would be a major help in studying the chemistry and properties of these important species.

MATERIALS AND METHODS

LFP Experiments. fs-Transient Absorption (fs-TA) Experiments. The fs-TA measurements were performed on the basis of a commercial femtosecond Ti/sapphire regenerative amplifier laser system and Helios Transient Absorption Spectrometer. A flow cell was used in order to prevent the accumulation of photodecomposition products. For the present experiments, the sample solution was excited by a 267 nm pump beam

(the third harmonic of 800 nm, the regenerative amplifier fundamental) and probed by a white light continuum produced from a one-dimensional movable CaF_2 plate pumped by the fundamental laser pulses (800 nm). The pump and probe laser beam spot sizes at the sample were about 500 and 200 μm, respectively. The detection signals (with and without 267 nm pump) were focused into an optics fiber coupled to a multichannel spectrometer with a CMOS sensor. The time delay between the pump and probe pulse was controlled by an optical delay line, and the instrument response time was ~200 fs. The fs-TA experiments were carried out for precursor **3** in neat MeCN and 1/1 H_2O/MeCN with a sample concentration of ~1 μM.

ps-Kerr-Gated-Time-Resolved Resonance Raman (ps-KTR3) Experiments. Briefly, the Ti/sapphire regenerative amplifier laser system was operated in picosecond mode with a 800 nm, ~1 ps, and 1 kHz output. Samples were pumped by a 267 nm pulse and probed with a 400 nm pulse. The 267 and 400 nm probe pulses were the third and second harmonics of the regenerative amplifier fundamental, respectively. The pump and probe pulse durations were ~1.5 ps; the pulse energies at the sample were 8−10 μJ. The pump and probe laser beams were lightly focused onto a flowing liquid sample, and the Raman scattering was collected via a backscattering configuration and then focused into the Kerr medium (CS_2 in a 1 mm thickness UV cell) placed at the other focus point of the ellipse. The Kerr medium was placed between a crossed polarizer pair with an extinction coefficient of ~104. The gating beam was polarized at 45° and focused to the Kerr medium with an adjusted intensity to create, in effect, a half-waveplate that rotates the polarization of the light from the sample, allowing it to be transmitted through a Glan Taylor polarizer for the duration of the induced anisotropy created by the femtosecond

gating pulse. The Raman light that passed through the second polarizer was focused into a monochromator and detected by a liquid N_2 cooled CCD. The wavenumber shifts of the resonance Raman spectra were calibrated using the known MeCN solvent Raman bands, and the spectra presented were obtained from subtraction of an appropriately scaled probe-before-pump spectrum from the corresponding pump−probe spectrum. The ps-KTR3 measurements were also carried out for BDP in 100% MeCN.

Product Studies. Product studies were performed with 5 mg of precursor **3** dissolved in 3 mL of solvent. The sample was degassed before beginning the photolysis, and the sample was irradiated with 254 nm UV light from a mercury vapor lamp for 1 h in a Rayonet photoreactor. The solvent was then removed, and a ^{1}H NMR spectrum was obtained. Thermolysis studies were performed similarly with 10 mg of precursor 3 and 10 mL of solvent refluxed for 1 h.

Computational Methods. For the computational studies, all of the molecular geometries were optimized at the B3LYP/CC-pVTZ level of theory.[32−34] The stationary points were found to have zero imaginary frequencies, and all energies contain a correction for the zero-point energy. Transition states were found to have one imaginary frequency that connected the starting material and product and included a PCM solvent model for water. The UV spectra were computed using TD-B3LYP/6-311+G(2d,p). The resonance Raman spectra were found using B3LYP/6-31+G(d,p) with a 400 nm incident beam, and all frequencies were scaled by 0.964.[35] All computations were done with Gaussian 09.[36]

Figure 7: Synthetic pathway for the formation of the tetrafluoroborate salts used for photolysis studies

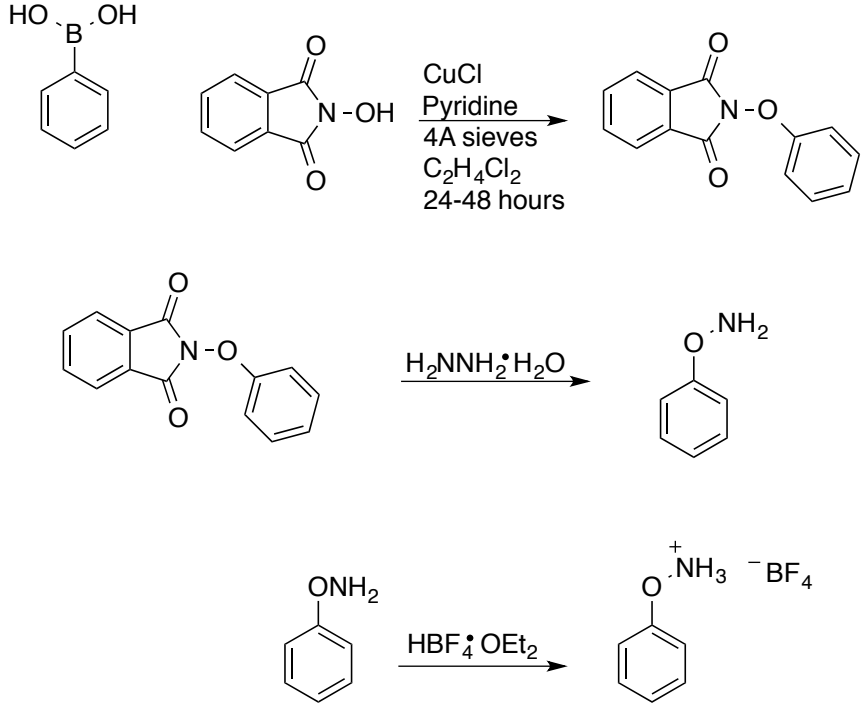

Synthesis of **3** (Figure 7). Compound **3** was made by a modified known procedure.[37] Synthesis of **N**-phenoxyphthalimide. 163 mg (1mmol, 1eq) of N hydroxyphthalimide, 99mg (1mmol, 1equiv) of CuCl, 244 mg (2 mmol, 2 equiv) of phenylboronic acid, and ~250 mg of 4. molecular sieves were added to a round bottom flask. 5 mL of 1,2-dichloroethane followed by 90 **µ**L (1.1 mmol, 1.1 equiv) of pyridine were added to the flask. The reaction was stirred overnight under air at ambient temperature. The reaction was monitored by TLC (75:25 Hexanes:Ethyl Acetate). The reaction was allowed to react for 24 hours and then the solvent was evaporated under reduced pressure. The product was separated by column chromatography (3:1 Hexanes:Ethyl Acetate). A white solid (N-phenoxyphthalimide) was collected and dried by high vacuum, to give 70% yield (168 mg), of the desired product. This product was then used for the next step in the synthesis. When this reaction was scaled up, the reaction took substantially longer. For example, whenever the reaction was run on 3 times the

scale, the reaction time was typically around 5 days before workup.

^{1}H NMR of the above N-phenoxyphthalimide

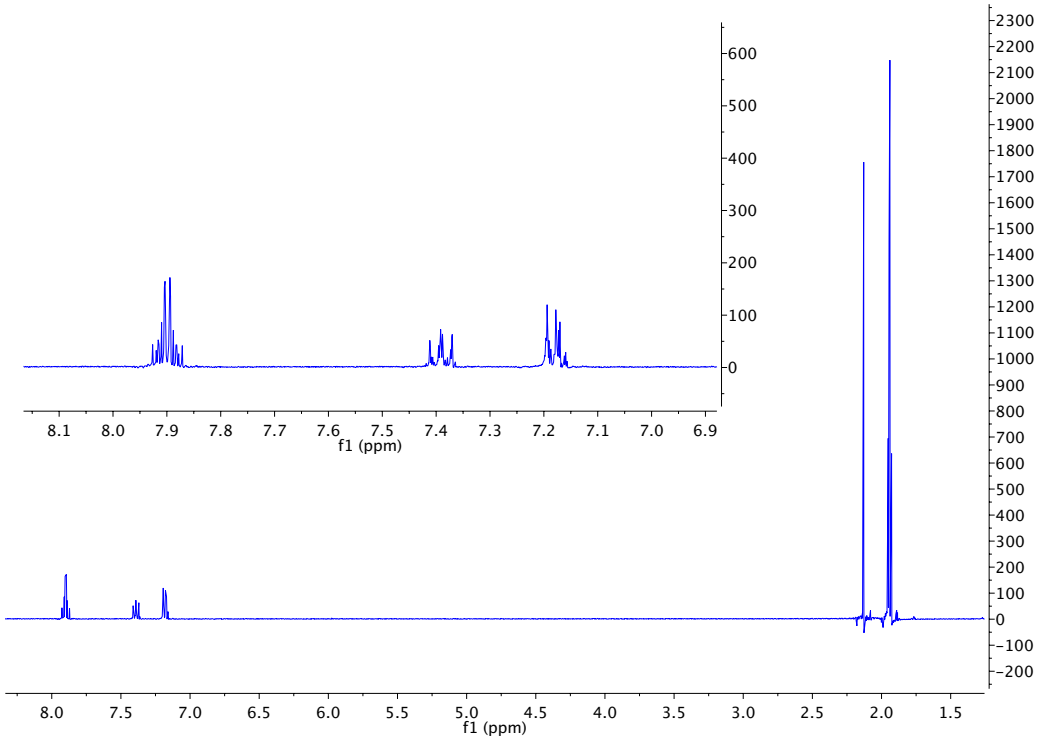

Synthesis of O-phenylhydroxylamine tetrafluoroborate **3**. 652 mg (2.73 mmol, 1 equiv) of N-phenoxyphthalamide was added to a flask containing 25 mL of 10% MeOH in CHCl3 and 0.401 mL (8.2 mmol, 3 equiv) of hydrazine monohydrate. A colorless solution was formed, which yielded a white precipitate over time. The reaction was monitored by TLC (75:25 Hexanes:Ethyl Acetate) and allowed to react overnight (12 hours). The filtered solid was then purified by column chromatography (75:25 Hexanes:Ethyl Acetate). The resulting product was dissolved in ether, to which HBF_4*OEt_2 (ca. 0.2 mL) was added until the TLC spot no longer moved. This signified the protonation of the hydroxylamine to the hydroxylamine tetrafluoroborate salt. This solution was then dried under reduced pressure to yield 155 mg of the desired salt. (155 mg, 29% yield). The product was reasonably stable stored in a freezer in the dark, but

over time decomposes to a colored solid with formation of ammonium ion evident by ^{1}H NMR.

^{1}H NMR of phenylhydroxylamine tetrafluoroborate

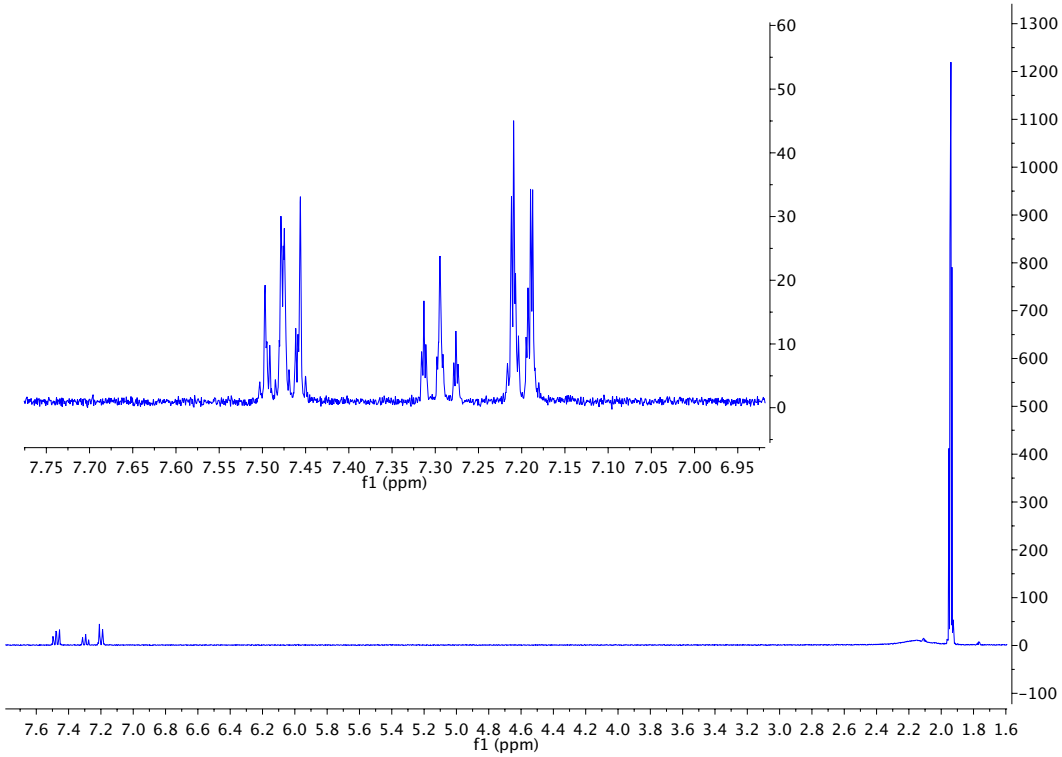

Sample product studies with identification of peaks

Photolysis of 3 in water

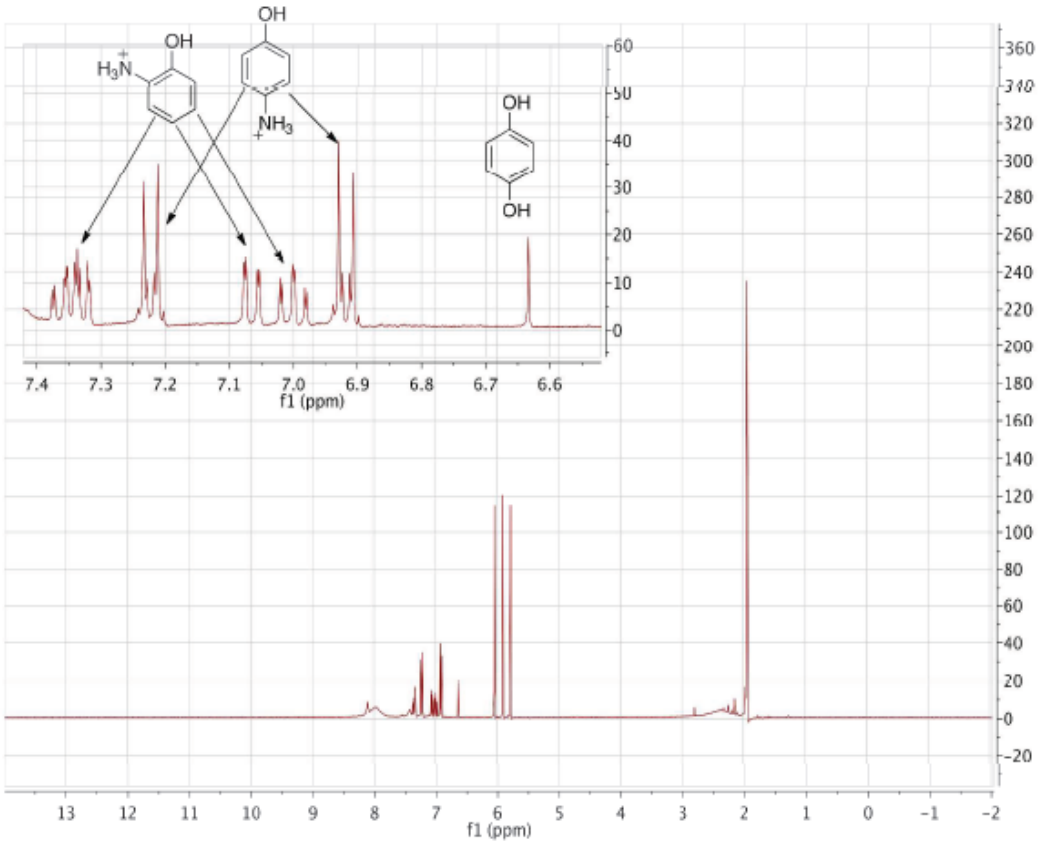

Photolysis of **3** in ACN

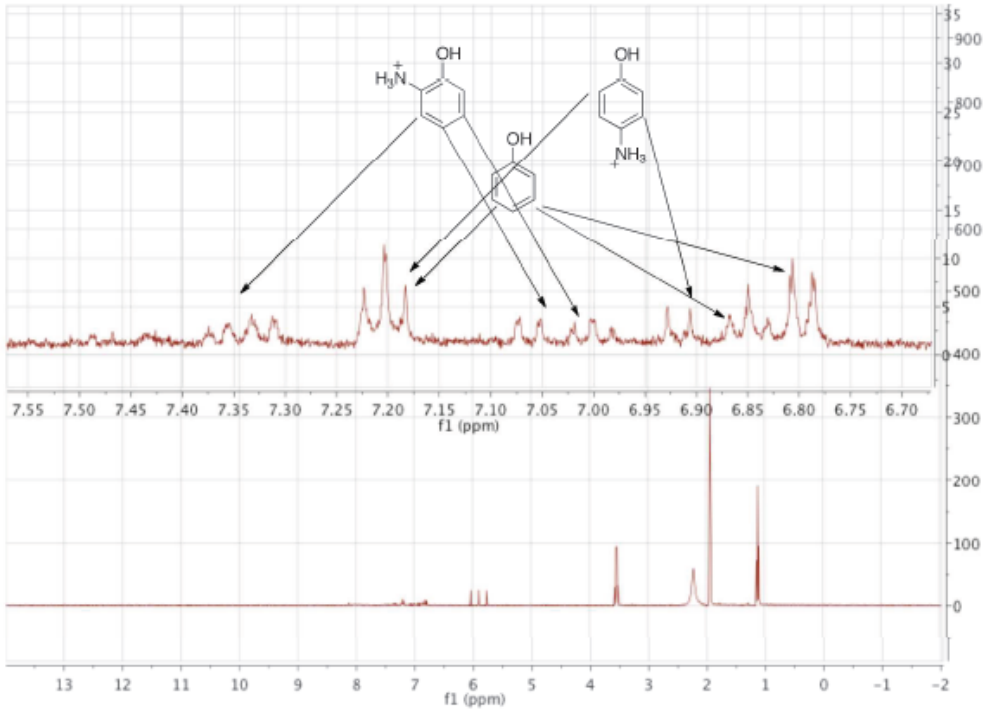

Photolysis of **3** in MeOH

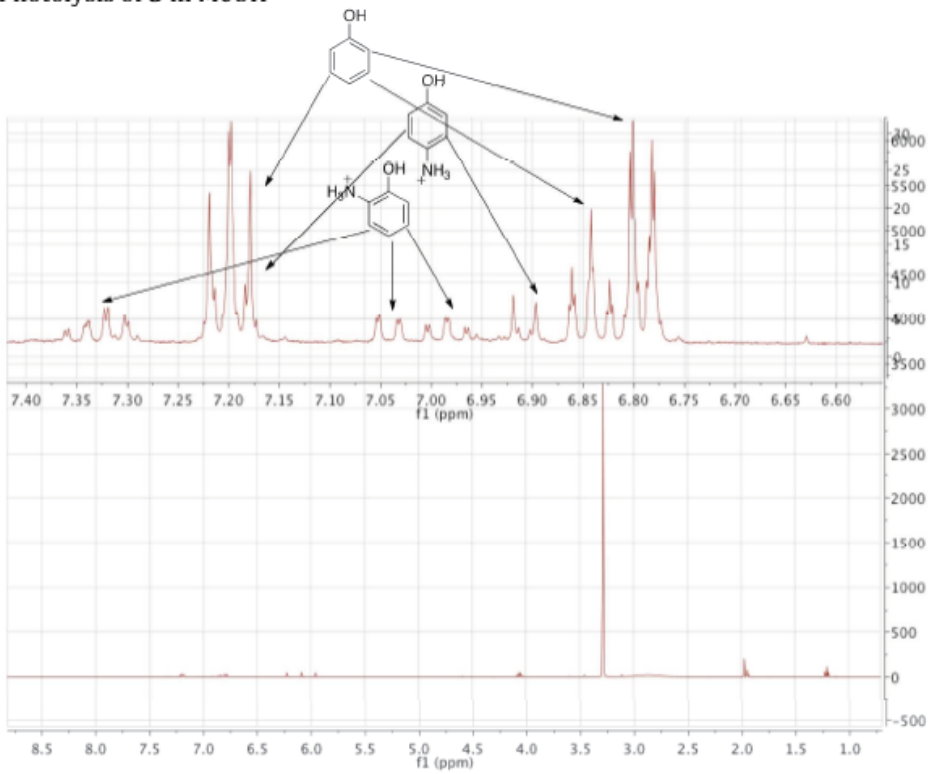

Photolysis of **3** in 1:1 MeOH/H_2O

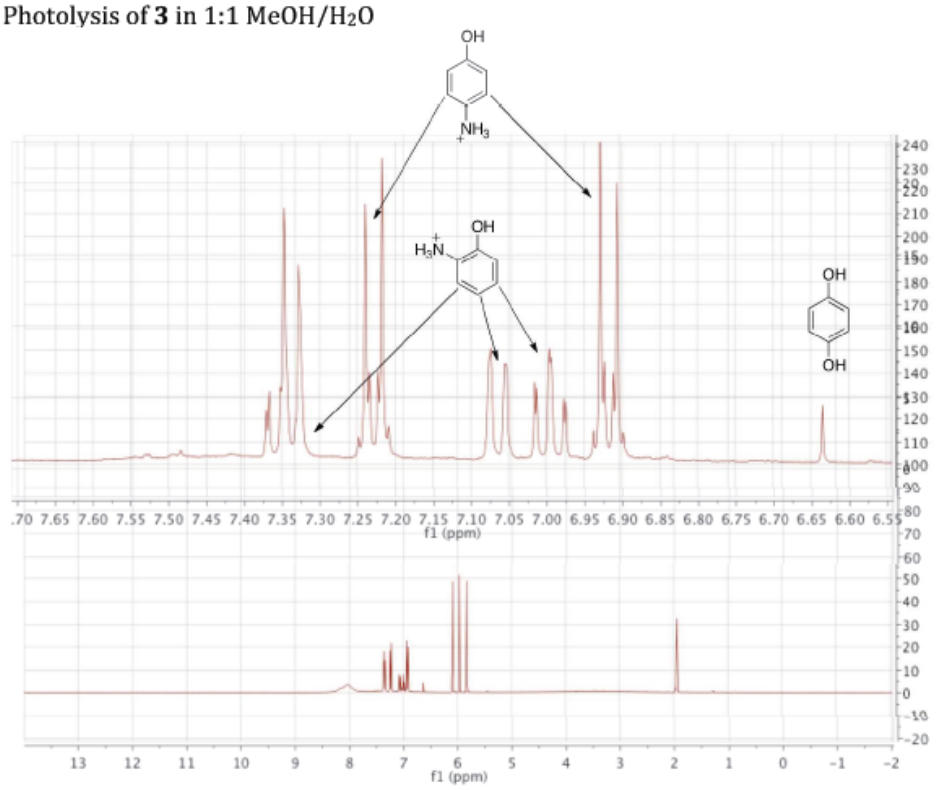

Photolysis of **3** in 1:1 ACN/H_2O

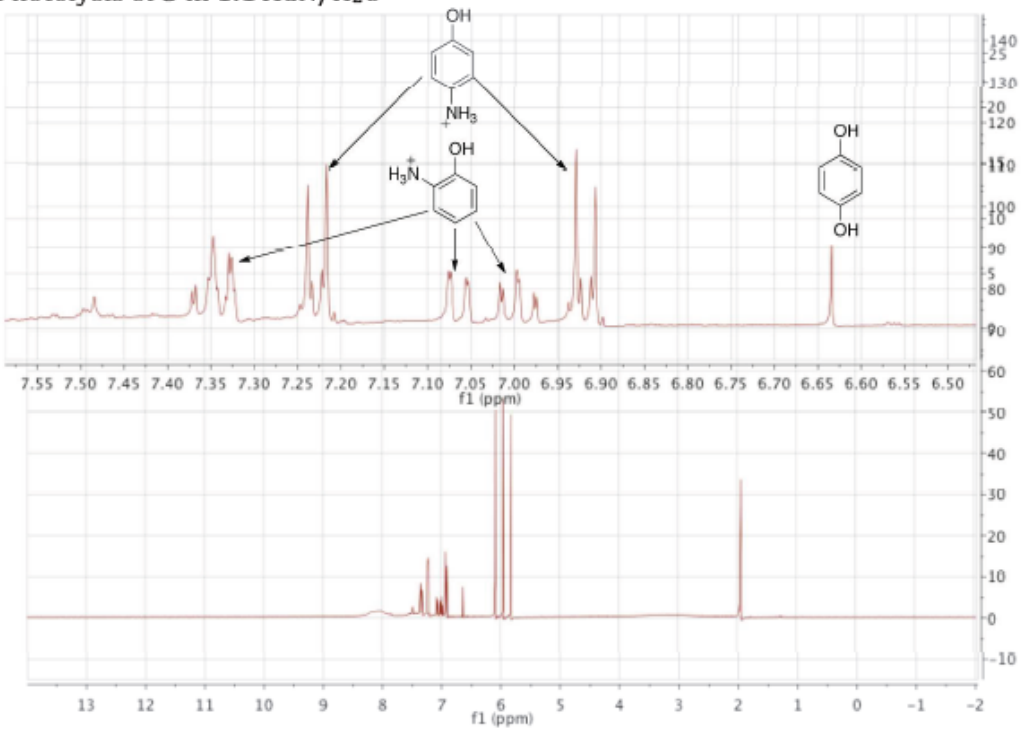

Thermolysis of **3** in H_2O

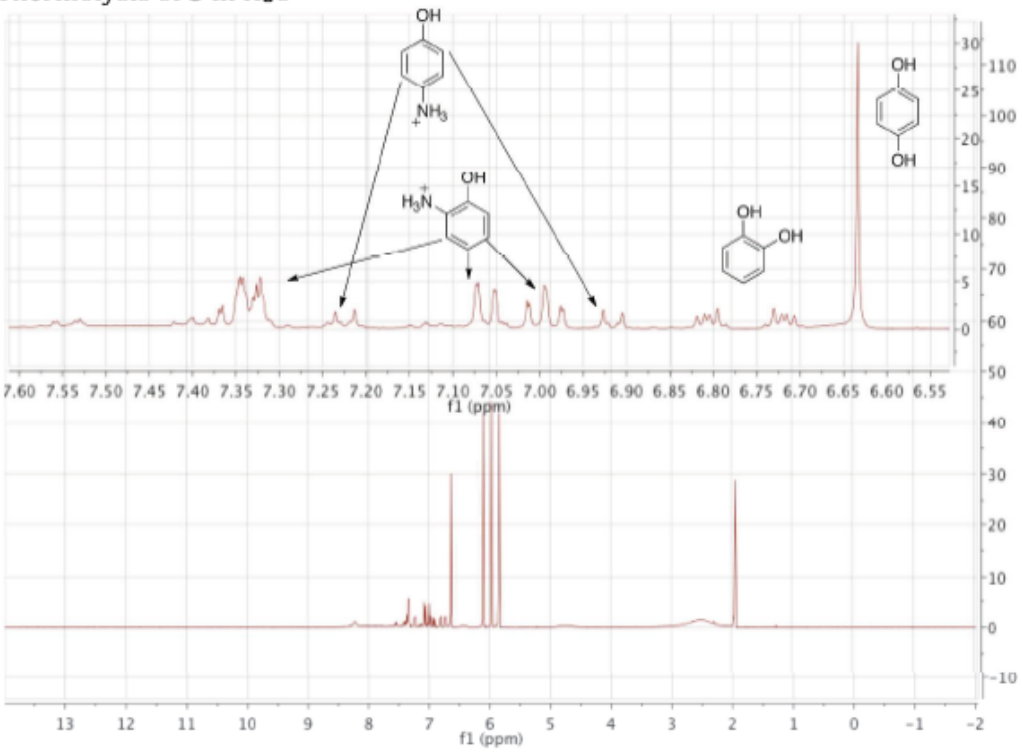

REFERENCES

(1) Zhang, Y.; Kubicki, J.; Wang, J.; Platz, M. S. *J. Phys. Chem. A* 2008, **112**, 11093.

(2) Zhang, Y.; Burdzinski, G.; Kubicki, J.; Platz, M. S. *J. Am. Chem. Soc.* 2008, **130**, 16134.

(3) Burdzinski, G. T.; Gustafson, T. L.; Hackett, J. C.; Hadad, C.M.; Platz, M. S. *J. Am. Chem. Soc.* 2005, **127**, 13764.

(4) Gritsan, N. P.; Tigelaar, D.; Platz, M. S. *J. Phys. Chem. A* 1999, **103**, 4465.

(5) Gritsan, N. P.; Gudmundsdottir, A. D. R.; Tigelaar, D.; Zhu, Z.; Karney, W. L.; Hadad, C. M.; Platz, M. S. *J. Am. Chem. Soc.* 2001, **123**, 1951.

(6) Wang, J.; Kubicki, J.; Platz, M. S. *Org. Lett.* 2007, **9**, 3973.

(7) Xue, J.; Luk, H. L.; Eswaran, S. V.; Hadad, C. M.; Platz, M. S. *J. Phys. Chem. A* 2012, **116**, 5325.

(8) Wang, J.; Burdzinski, G.; Zhu, Z.; Platz, M. S.; Carra, C.; Bally, T. *J. Am. Chem. Soc.* 2007, **129**, 8380.

(9) Siuzdak, G.; North, S.; BelBruno, J. J. *J. Phys. Chem.* **1991**, *95*, 5186.

(10) Hwang, W. G.; Kim, M. S.; Choe, J. C. *J. Phys. Chem.* 1996, **100**, 9227.

(11) Kosmidis, C.; Ledingham, K. W. D.; Kilic, H. S.; McCanny, T.; Singhal, R. P.; Langley, A. J.; Shaikh, W. *J. Phys. Chem. A* 1997, **101**, 2264.

(12) Syage, J. A.; Steadman, J. *J. Phys. Chem.* 1992, **96**, 9606.

(13) Novak, M.; Glover, S. A. *J. Am. Chem. Soc.* 2004, **126**, 7748.

(14) Novak, M.; Brinster, A. M.; Dickhoff, J. N.; Erb, J. M.; Jones, M.P.; Leopold, S. H.; Vollman, A. T.; Wang, Y. T.; Glover, S. A. *J. Org. Chem.* 2007, **72**, 9954.

(15) Novak, M.; Glover, S. A. *J. Am. Chem. Soc.* 2005, **127**, 8090.

(16) Novak, M.; Poturalski, M. J.; Johnson, W. L.; Jones, M. P.; Wang, Y. T.; Glover, S. A. *J. Org. Chem.* 2006, **71**, 3778.

(17) Wang, Y.-T.; Jin, K. J.; Leopold, S. H.; Wang, J.; Peng, H.-L.; Platz, M. S.; Xue, J.; Phillips, D. L.; Glover, S. A.; Novak, M. *J. Am. Chem. Soc.* 2008, **130**, 16021.

(18) Wang, Y. T.; Wang, J.; Platz, M. S.; Novak, M. *J. Am. Chem. Soc.* 2007, **129**, 14566.

(19) Winter, A. H.; Thomas, S. I.; Kung, A. C.; Falvey, D. E. *Org. Lett.* 2004, **6**, 4671.

(20) Baptista, J. L.; Burrows, H. D. *J. Chem. Soc., Faraday Trans. 1* 1974, **70**, 2066.

(21) Tripathi, G. N. R.; Schuler, R. H. *J. Chem. Phys.* 1984, **81**, 113.

(22) Land, E. J.; Porter, G.; Strachan, E. *Trans. Faraday Soc.* 1961, **57**, 1885.

(23) Shindo, H.; Hiraishi, J. *Chem. Phys. Lett.* 1981, **80**, 238.

(24) Gritsan, N. P.; Likhotvorik, I.; Zhu, Z.; Platz, M. S. *J. Phys. Chem. A* 2001, **105**, 3039.

(25) Delamere, C.; Jakins, C.; Lewars, E. *J. Mol. Struct. (THEOCHEM)* 2002, **593**, 79.

(26) Xue, J.; Luk, H. L.; Eswaran, S. V.; Hadad, C. M.; Platz, M. S. *J. Phys. Chem. A* 2012, **116**, 5325.

(27) Abramovitch, R. A.; Alvernhe, G.; Bartnik, R.; Dassanayake, N.L.; Inbasekaran, M. N.; Kato, S. *J. Am. Chem. Soc.* 1981, **103**, 4558.

(28) Abramovitch, R. A.; Alvernhe, G.; Inbasekaran, M. N. *Tetrahedron Lett.* 1977, 1113.

(29) Abramovitch, R. A.; Inbasekaran, M.; Kato, S. *J. Am. Chem. Soc.* 1973, **95**, 5428.

(30) Endo, Y.; Shudo, K.; Okamoto, T. *J. Am. Chem. Soc.* 1982, **104**, 6393.

(31) Shudo, K.; Orihara, Y.; Ohta, T.; Okamoto, T. *J. Am. Chem. Soc.* 1981, **103**, 943.

(32) Lee, C.; Yang, W.; Parr, R. G. *Phys. Rev. B* 1988, **37**, 785.

(33) Becke, A. D. *Phys. Rev. A* 1988, **38**, 3098.

(34) Becke, A. D. *J. Chem. Phys.* 1993, **98**, 5648.

(35) Johnson, R. D., III. NIST Computational Chemistry Comparison and Benchmark Database, NIST Standard Reference Database Number 101, Release 15b, August 2011; http://cccbdb.nist.gov/.

(36) Frisch, M. J., et al. *Gaussian09, version A.02*; Gaussian Inc., Pittsburgh, PA, 2009.

(37) Petrassi, H. M.; Sharpless, K. B.; Kelly, J. W. *Org. Lett.* 2000, 3, 139.

CHAPTER 3
HETEROARYL OXENIUM IONS HAVE DIVERSE AND UNUSUAL LOW-ENERGY ELECTRONIC STATES

Taken in part from:
Hanway, P. J.; Winter, A. H. *The Journal of Physical Chemistry A* **2012**, *116*, 9398.

INTRODUCTION

Recently, the electronic state energies of phenyl oxenium ions and simple derivatives were computed using the CASPT2//CASSCF computational method.[1] These computational studies suggested that oxenium ions undergo large changes in the electronic state orderings by changing the substituent attached to the formally positive oxygen. For instance, the simplest oxenium ion, OH^+, has a triplet ground state with a gap of 54 kcal/mol to the lowest energy singlet state.[2] Substituting the hydrogen with a phenyl ring leads to the lowest-energy state being the closed-shell singlet ground state.[1] The singlet ground state of phenyl oxenium ion is supported by both photoelectron spectroscopy and high-level computational methods. In particular the parent phenyl oxenium ion (Ph-O+) was computed by us to have a singlet−triplet gap (ΔE_{ST}) of −22.1 kcal/mol (CASPT2/pVTZ, a negative value indicates a singlet ground state);[1] this value compares favorably with the value of −19.8 kcal/mol found from photoelectron spectroscopy experiments.[3] This study also provided evidence that simple ring substituents could lead to significant changes in the ΔE_{ST}. [1] For example, m-aminophenyl oxenium ion was computed to have essentially degenerate singlet and triplet states. Whereas oxenium ions are common reactive intermediates that are important to a diverse group of chemists, the properties, electronic states, and reactivities of these species are

poorly understood. Furthermore, the exuberant change of ca. 70 kcal/mol in the ΔE_{ST} on substituting the hydrogen for a phenyl ring at the oxenium center suggests that the ground-state configurations of these ions are highly sensitive to the substituent.

In this study, we computed the electronic states of heteroaryl oxenium ions using CASPT2//CASSCF computations as well as high-level single-reference methods (CCSD(T), CBS-Q) for ions found to be compatible with a single-reference approach. From these computations, we find that heteroaryl oxenium ions have a number of low-energy electronic states. The lowest energy configuration of these heteroaryl oxenium ions can be the open-shell singlet, closed-shell singlet, or triplet configuration. Therefore, these heteroaryl oxenium ions may prove to be interesting test cases for studying the spin-selective reactivity of oxenium ions.

COMPUTATIONAL METHODS

The geometries and energies for the different electronic states of the heteroaryl oxenium ions reported in this article were computed using the CASPT2//CASSCF methodology. This methodology has proven to be robust for obtaining accurate energies with appropriate active space selection for excited electronic states.[4−6] It is worth noting that our calculation of the phenyl oxenium ion (Ph-O+) using this same method gives a ΔE_{ST} of −22.1 kcal/mol,[1] in good agreement with experiment (−19.8 kcal/mol).[3] Additionally, our benchmarks with this method and software for the isoelectronic phenyl nitrene are +17.2 and +31.4 kcal/mol for the gaps between the $^3A_2$-$^1A_2$ and the $^3A_2$-$^1A_1$ states[21] (experimental values for these gaps are 18 and 30 kcal/mol, respectively[7−9]). These benchmarks for related species give us confidence in this computational method for the systems described here for which experimental values have not been reported.

Additionally, for those systems that are computed to have lowest energy singlet states that are closed shell and essentially single-reference, we used high-level single reference methods to corroborate the CASPT2 results (CCSD(T) and CBS-Q), for which we found good agreement with the CASPT2 results. For the CASPT2/CASSCF computations, the active space orbitals included all of the π and π* orbitals, the in-plane oxygen p orbital, and any lone pair electrons and σ orbitals on nitrogen atoms. Therefore, all of the molecular geometries of the electronic states of 2-, 3-, and 4-pyridinyl oxenium ions were computed at the CASPT2(10,9)/pVTZ//CASSCF(10,9)/pVTZ level. The basis set employed was the flexible ANO-L basis set of Widmark et al., which is of polarized valence triple-ζ (pVTZ) quality.[10] All active space orbitals were inspected using the Molden software. The pyrimidinyl and pyrizidinyl oxenium ions, which have an additional lone pair of electrons and orbital in the active space, were computed at the CASPT2(12,10)//CASSCF(12,10) level of theory.[11] Except where noted, all of these optimized structures were found to have zero imaginary frequencies, and all of the energies contained a correction for the zero point energy (unscaled). Optimizations were initially carried out using the highest molecular symmetry ($\mathbf{C_{2v}}$ or $\mathbf{C_s}$) possible. For those states that had imaginary frequencies under high symmetry, optimizations were performed under reduced symmetry constraints. To keep the state under discussion clear, we designate the states using the irreducible representations for that configuration at the highest possible molecular symmetry ($\mathbf{C_{2v}}$ or $\mathbf{C_s}$), even in cases in which the optimized structure for that electron configuration is nonplanar. (These lower symmetry geometries are designated with a * in the Tables.) In the few cases where the lone pair of electrons does not contribute significantly (e.g., electron population ~2), the orbital containing the

lone pair was sometimes replaced with a **σ** orbital of identical symmetry, also with an occupation of ~2. All CASPT2/CASSCF calculations were performed using the MOLCAS 7.4 software suite.[12,13] All CCSD(T), B3LYP, and CBS-Q calculations were computed using Gaussian 09.[14]

RESULTS AND DISCUSSION

The degenerate p orbitals on OH^+ lead to the triplet being the ground state following a molecular orbital extension of Hund's rule. In contrast, substituting the hydrogen for a phenyl ring strongly breaks the degeneracy of the frontier orbitals in the phenyl oxenium ion and leads to the ground state being a singlet ($^1A_1$) with the lowest triplet state ($^3A_2$) 20 kcal/mol higher in energy. Intuitively, one expects substituting carbons for nitrogen in the aryl ring would shift the ΔE_{ST} back toward the triplet because the electron-donating capacity of the ring is reduced, leading to poorer energy match and poorer mixing of the ring **π** orbitals with the out-of-plane p orbital on the oxenium center. This is indeed the case. Figure 1 depicts the overall ΔE_{ST} of heteroaryl oxenium ions computed in this study and compares these values to the parent phenyl oxenium ion. It is clear that the addition of nitrogen into the aromatic ring favors the triplet when compared with the phenyl oxenium ion.

Figure 1. Computed ΔE_{ST} of the phenyloxenium ions and heterocyclic oxenium ions.

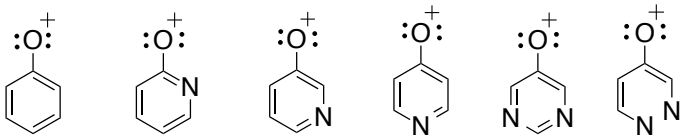

Compound Number	**1**	**2**	**3**	**4**	**5**	**6**
E_{ST} (B3LYP/cc-PVTZ)	-13.5	-1.4	-3.8	+0.9	--	--
E_{ST} (CASPT2/pVTZ)	-22.1	-16.4	-19.2	-3.4	-0.4	-1.3
E_{ST} (CBS-Q)	-20.5	-14.1	-15.6	-6.5	--	--
E_{ST} (CCSD(T)/cc-pVTZ// CCSD/cc-pVDZ)	-16.5	-10.6	-15.4	-4.4	--	--

2-Pyridinyl Oxenium Ion 2 and 3-Pyridinyl Oxenium Ion 3 Have Only Slightly Perturbed Energetic Orderings from the Phenyl Oxenium Ion 1.

For each ion, the lowest energy configuration for each irreducible representation at its highest molecular symmetry was computed. Most of these states can be reasonably well-represented as a single determinant, and thus the electronic configuration of the major determinant is depicted in Figure 2 to help guide the discussion.

Figure 2. Approximate schematic configurations of the singlet and triplet irreducible representations ($\mathbf{C_s}$) of the 2-pyridinyl oxenium ion **2** (top). Heavy atom-heavy atom bond lengths (Å) for irreducible representations of **2** ($\mathbf{C}_s$, CASSCF(10,9)/pVTZ) (bottom).

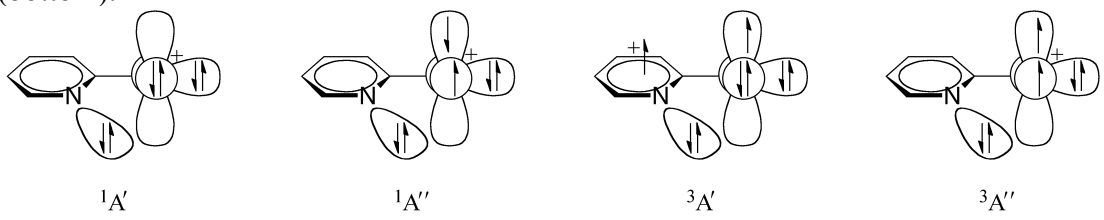

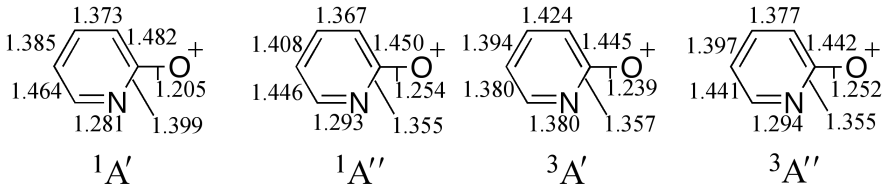

Table 1. Energies of the Lowest Irreducible Representations of the 2-Pyridinyl Oxenium Ion **2**[a] irreducible representation ($\mathbf{C_s}$) relative energy adiabatic (vertical), kcal/mol

Irreducible Representation (C_s)	Relative energy adiabatic (vertical), kcal/mol
$1^1A'$	0
$1^1A''$	23.8
$1^3A'$	36.3† (49.0)
$1^3A''$	16.4

[a]† indicates that an imaginary frequency was encountered upon optimization under symmetry.

As shown in Table 1, the ΔE_{ST} ($^1A'$-$^3A''$) of the 2-pyridinyl oxenium ion **2** is computed to have a gap of 16.4 kcal/ mol between the closed-shell singlet and an n,π^* triplet state. Therefore, there can be little doubt that the ground state of the 2-pyridinyl oxenium ion is the closed-shell singlet state. A very short C−O bond length of 1.205 Å (Figure 2) for the ground singlet state implicates a quinoidal structure with significant charge on the carbon para to the oxygen (e.g., a structure resembling an azacyclohexadienonyl cation).

Table 2. Energy of the Irreducible Representations of the 3-Pyridinyl Oxenium Ion **3**[a] irreducible representation ($\mathbf{C_s}$) relative energy (adiabatic) kcal/mol

Irreducible Representation (C_s)	Relative energy adiabatic
$1^1A'$	0
$1^1A''$	22.8
$1^3A'$	41.9
$1^3A''$	19.2

[a]* designates a lower-symmetry geometry.

Figure 3. Approximate schematic configurations of the singlet and triplet irreducible representations ($\mathbf{C_s}$) of the 3-pyridinyl oxenium ion **3** (top). Heavy atom-heavy atom bond lengths (Å) for irreducible representations of **3** ($\mathbf{C_s}$, CASSCF(10,9)/pVTZ) (bottom).

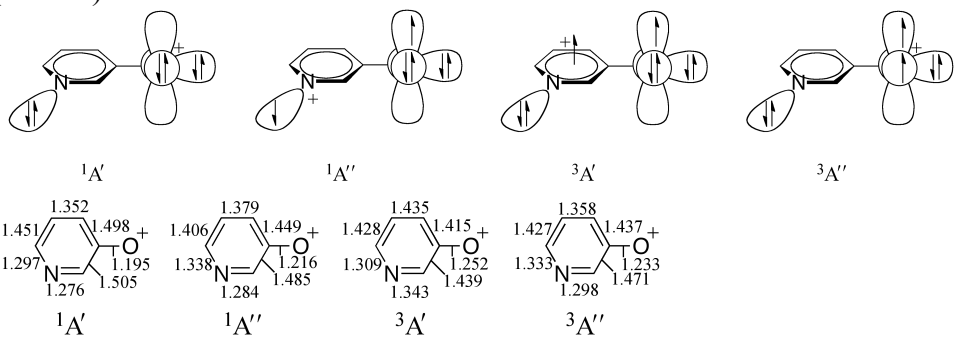

These two states are identical to the lowest energy states for the phenyl oxenium ion but with a reduced energy gap of 6 kcal/mol. (The ΔE_{ST} of phenyl oxenium ion is −22 kcal/mol between $^1A_1$ and $^3A_2$ at the same level of theory.) Like the 2-pyridinyl oxenium ion **2**, as shown in Table 2, the ΔE_{ST} of the 3-pyridinyl oxenium ion **3** is computed to be 19.2 kcal/mol ($^1A'$-$^3A''$). As with its isomer **2**, this value leaves little doubt that the singlet state is the ground state for this ion. The $^3A''$ state derives from promoting an electron from an oxygen lone pair to the formally oxygen-centered π* orbital (Figure 3). Because 3-pyridinyl oxenium has the nitrogen in the meta position to the oxenium center, it would be expected that this heteroaryl oxenium ion would vary the least from the phenyl oxenium ion because it lacks a resonance structure that would formally place the positive charge on the nitrogen. Indeed, the ordering of the three lowest electronic states is the same at the phenyl oxenium ion (ground state singlet < triplet < open-shell singlet), and even the energy gaps are only slightly perturbed. As with the 2-pyridnyl oxenium ion **2** the 3-pyridinyl oxenium ion **3** has a short C−O bond distance of 1.195 Å showing a quinodal structure. In contrast with the 2- and 3-pyridinyloxenium Ions, the 4-pyridinyl oxenium Ion has a significantly smaller Singlet−Triplet gap than the parent phenyl

Table 3. Energies of the Lowest Irreducible Representations of the 4-Pyridinyl Oxenium Ion **4**[a] irreducible representation (**C_{2v}**) relative energy adiabatic (vertical) kcal/mol

Irreducible Representation (C_{2v})	Relative energy adiabatic (vertical)
1^1A_1	0
1^1A_2	22.36† (24.78)
1^1B_1	10.59† (9.67)
1^1B_2	33.52
1^3A_1	60.08
1^3A_2	13.43
1^3B_1	3.41
1^3B_2	15.07

[a]† indicates that an imaginary frequency was encountered upon optimization under symmetry.

Figure 4. Approximate schematic configurations of the singlet and triplet irreducible representations ($\mathbf{C_{2v}}$) of 4-pyridinyl oxenium ion **4** (top). Heavy atom-heavy atom bond lengths (Å) for irreducible representations of **4** ($\mathbf{C_{2v}}$, CASSCF(10,9)/pVTZ) (bottom).

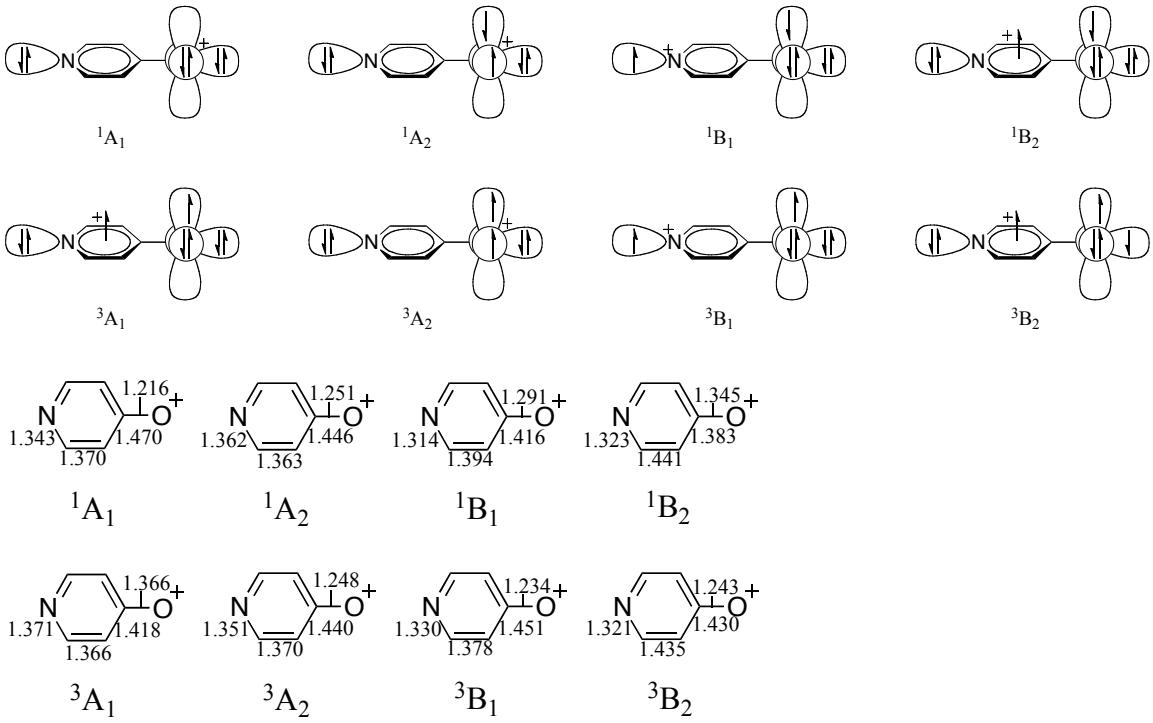

oxenium Ion. As shown in Table 3, the singlet−triplet gap of the 4-pyridinyl oxenium ion **4** is computed to be −3.4 kcal/mol ($^1A_1$-$^3B_1$). Interestingly, the lowest energy triplet state for this ion is not the typical oxygen-centered n,$\boldsymbol{\pi}$* triplet state seen with the phenyl oxenium ion and the 2- and 3-pyridinyl oxenium ion but is better described as an n,$\boldsymbol{\pi}$* triplet nitrenium ion, with the ring nitrogen **n** electron promoted to the $\boldsymbol{\pi}$* orbital (Figure 4). Both the closed-shell singlet and the lowest energy triplet state have C−O bond lengths that are very short (1.216 and 1.234 Å, respectively), suggesting quinoidal nitrenium ion character for both the singlet and triplet states. In some cases indicated with a † in the Tables, optimization under symmetry gives imaginary frequencies. Unfortunately, without symmetry, optimizing a particular excited-state root when there are numerous similar-energy roots is a challenging problem. Despite numerous attempts

with varying input geometries, state averaging, and manual single-step optimization approaches, we were unable to achieve an optimized geometry for these states.

Attempting to optimize these excited states without symmetry led to problems with root switching upon optimization, wherein the optimization would reach a conical intersection and convergence problems or root switching would be encountered. For the optimizations of the excited state roots that were unsuccessful, we report the energy for this state at the geometry optimized under symmetry as well as the vertical energy with CASPT2 from the ground-state optimized geometry (in parentheses). Fortunately, because these are excited states at the CASSCF level, these states are probably less chemically relevant for the 4-pyridinyl oxenium ion.

Absolute Energies Indicate Singlet Destabilization is the Dominant Factor for Changing the $\mathbf{\Delta}E_{ST}$ for 2, 3, and 4. A natural question is whether the difference in singlet−triplet gaps for the 2-, 3-, and 4-pyridinyl oxenium ions can be explained by stabilization/destabilization of the triplet state, stabilization/destabilization of the singlet state, or a combination both. Because these ions are isomers of each other the absolute energies can be compared to provide insight into this question. Absolute energies indicate that the singlet state of the 4-pyridinyl oxenium ion 4 is 19 kcal/mol less stable than the singlet state of 3-pyridinyl oxenium ion 3, whereas the triplet state shows only a 3.5 kcal/mol destabilization. Therefore, the reason 4 has a nearly zero singlet−triplet gap compared with 3 is primarily due to ion 4 having a considerably destabilized singlet state. When comparing the 2- and 4-pyridinyl oxenium ions, the singlet state was more stable by a remarkable 67 kcal/ mol, but this was offset by the triplet being stabilized by 53 kcal/mol. We attribute this stabilization of **2** due to the ability of the oxenium ion to

delocalize the positive charge on a less electronegative para carbon rather than a para nitrogen or a carbon adjacent to nitrogen. However, again it is seen that the singlet state destabilization is the major factor in altering the ΔE_{ST}.

Pyrimidinyl Oxenium Ion May Have a Remarkable Open-Shell Singlet Ground State.

As shown in Table 4, the ΔE_{ST} of the pyrimidinyl oxenium ion **5** is essentially zero. Therefore, there is little certainty as to whether the $^1A_2$ or the $^3A_2$ state is the ground state of the pyrimidinyl oxenium ion. Unfortunately, we were not able to obtain the optimized structure of the open-shell $^1A_2$ state.

Table 4. Energies of the Lowest Irreducible Representations of the Pyrimidinyl Oxenium Ion 5[a,b,c] irreducible representation ($\mathbf{C_{2v}}$) relative energy adiabatic (vertical) kcal/mol.

Irreducible Representation (C_{2V})	Relative energy adiabatic (vertical)
1^1A_1	5.42
1^1A_2	-.35† (0.98)
1^1B_1	56.97
1^1B_2	77.31
1^3A_1	73.73
1^3A_2	0
1^3B_1	56.66† (62.60)
1^3B_2	64.73

[a]An expanded (12,12) active space was needed to achieve convergence. [b]† indicates that an imaginary frequency was encountered upon optimization under symmetry. [c]* designates a lower-symmetry geometry.

Optimization of this irreducible representation under symmetry leads to an imaginary frequency. In a broken molecular symmetry calculation of this state, CASPT2 places the $^1A_2$ state as the ground state, but it is an excited-state root at the CASSCF level of theory. Our optimization suffered from intractable root switching problems upon optimization, as described above due to a near-degeneracy with the closed-shell singlet state at the CASSCF level. However, inspection of the energy of the symmetry-optimized structure as well as the vertical energy from the closed-shell singlet state shows that the

Figure 4. Approximate schematic configurations of the singlet and triplet irreducible representations ($\mathbf{C_{2v}}$) of Pyrimidinyl oxenium ion **4** (top). Heavy atom-heavy atom bond lengths (Å) for irreducible representations of **5** ($\mathbf{C_{2v}}$, CASSCF(12,10)/pVTZ) (bottom).

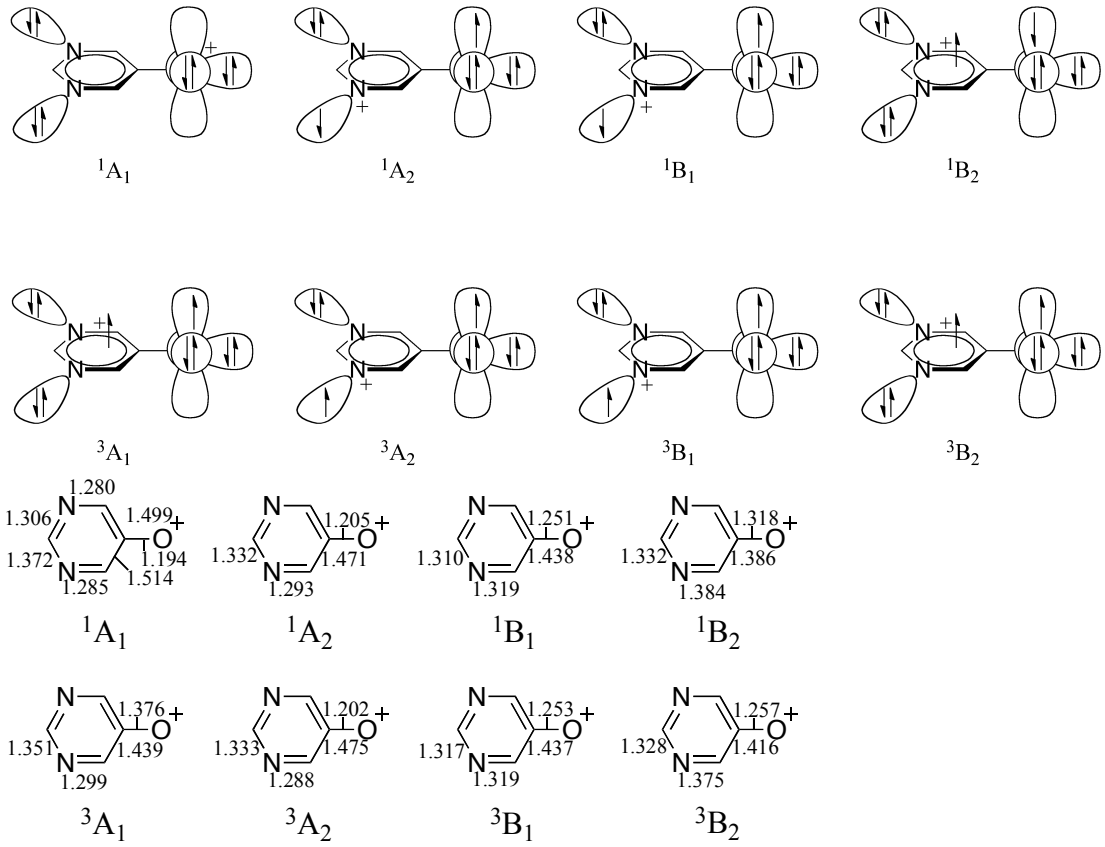

energy is similar to the $^3A_2$ state, although the open-shell singlet state is likely to be lower in energy because it is computed to be slightly lower in energy even without a fully optimized geometry. The significance of having the $^1A_2$ state lower than the $^1A_1$ state suggests that this ion may have an open-shell singlet ground state, quite unusual indeed. As seen in Figure 5, both the $^1A_2$ and $^3A_2$ states can be conceptually derived by starting with the closed-shell singlet and promoting an electron from the nitrogen lone pair to the oxygen π* orbital. In most cases, ground-state singlet molecules are closed shell, but if the frontier orbitals approach each other in energy then it is possible for an open-shell singlet to be the ground state. Typically, molecules that have lowest energy singlet states that are open-shell have triplet ground states due to the favorable exchange energy

favoring the triplet given equal orbital occupation. However, the open-shell singlet state can become the ground state if the exchange energy is small and higher order correlation favors the singlet over the triplet. The possibility of an open-shell singlet ground state for this ion makes it particularly intriguing for experimental study because there are few examples of ground-state open-shell singlet states for reactive intermediates[15−18] and the reactivity of open-shell singlet species is not well understood. The short C−O bond length (1.914 Å) shows its quinoidal character placing the positive charge on the carbon para to the oxygen.

Electronic State Orderings of the Pyrizidinyl Oxenium Ion 6 Show a Near-Triple Degeneracy in Electronic States.

As shown in Table 5, the ΔE_{ST} of the pyrizidinyl oxenium ion **6** is computed to be −1.3 kcal/mol. Therefore, as with the pyrimidinyl oxenium ion, there can be little certainty as to whether the $^1A'$ or $_3A''$ state is the ground state of the pyrizidinyl oxenium ion.

Table 5. Energies of the lowest Irreducible Representations of the Pyrizidinyl Oxenium Ion **6**[a,b] irreducible representation (**C_s**) relative energy adiabatic (vertical) kcal/mol

Irreducible Representation (Cs)	Relative energy adiabatic (vertical)
$1^1A'$	0
$1^1A''$	3.88† (3.87)
$1^3A'$	9.51
$1^3A''$	1.34

[a]† indicates that an imaginary frequency was encountered upon optimization under symmetry. [b]* designates a lower-symmetry geometry.

Indeed, with the open-shell ($^1A''$) state calculated to be only 3.9 kcal/mol higher in energy than the closed-shell ($^1A'$) state, it is uncertain if the closed shell is actually the lowest energy singlet state. It should be noted that the lone pair orbitals of the two adjacent nitrogens overlap, as inspection of the orbitals shows that there is a **"**bonding**"** and **"**antibonding**"** set of lone pair orbitals. Therefore, whereas Figure 6 shows the

Figure 6. Approximate schematic configurations of the singlet and triplet irreducible representations ($\mathbf{C}_s$) of pyrizidinyl oxenium ion **6** (top). Heavy atom-heavy atom bond lengths (Å) for irreducible representations of **6** ($\mathbf{C}_s$, CASSCF(12,10)/pVTZ) (bottom).

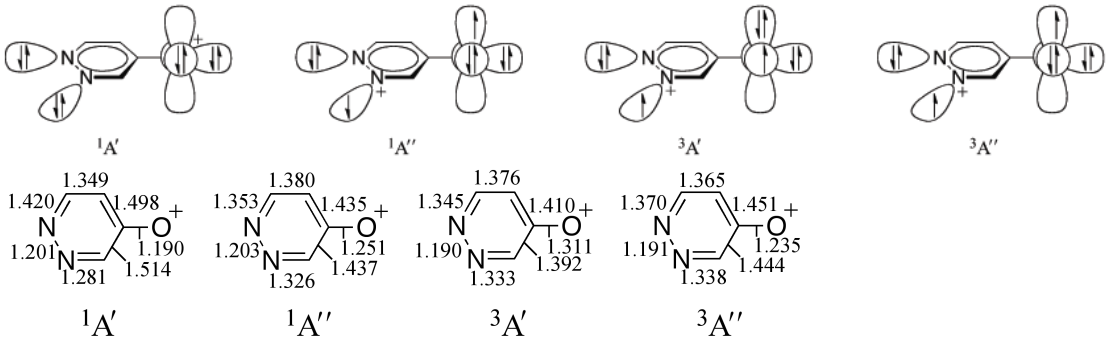

promotion of the electron from the meta nitrogen, it is better to ascribe this electron as originating from the **"**bonding**"** pair of electrons, which has amplitude on both ring nitrogens. As with the 4-pyridinyl oxenium ion **4**, the closed shell singlet is likely destabilized because it has a quinoidal structure that places the positive charge on the electronegative nitrogen.

High-Level Single-Reference Computations Corroborate CASPT2 Singlet− Triplet Gaps for Ions with a Lowest-Energy Singlet State That Are Single-Reference and Closed-Shell.

For ions with lowest-energy singlet states that were found to be essentially single-determinantal by CASSCF, we performed additional CCSD(T), CBS-Q, and B3LYP computations to obtain the singlet−triplet gaps shown in Figure 7. These included calculations using these methods for ions **2**, **3**, and **4**. (Ions 5 and 6 probably have an open-shell singlet ground state, or near-degenerate open-shell singlet states, and so are not amenable to calculation by single reference methods.) Our previous report on the phenyl oxenium ion showed that whereas B3LYP computed the ΔE_{ST} of phenyl oxenium to be −13.5 kcal/mol, CBS-Q and CCSD(T)/cc-PVDZ compute the singlet−triplet gap of phenyl oxenium ion to be −20.5 and −16.5 kcal/mol, respectively, in good agreement

with experiment (−19.8 kcal/mol). As in our previous study, B3LYP performs very poorly here for **2** and **3** compared with the CASPT2, CBS-Q, or CCSD(T) computations, underestimating the singlet energy by >10 kcal/mol. However, the CCSD(T)/cc-PVDZ computations as well as the CBS-Q computations are in good agreement with the CASPT2 results, differing by <5 kcal/mol for both species. This agreement among these best methods increases our confidence in the quantitative validity of these CASPT2 computations reported herein.

Figure 7: Calculated ΔE_{ST} of the phenyloxenium ion and heteroaryl oxenium ions.

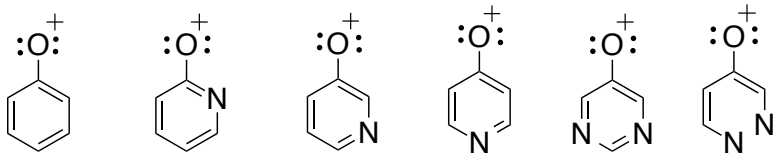

Compound Number	**1**	**2**	**3**	**4**	**5**	**6**
E_{ST} (B3LYP/cc-PVTZ)	-13.5	-1.4	-3.8	+0.9	--	--
E_{ST} (CASPT2/pVTZ)	-22.1	-16.4	-19.2	-3.4	-0.4	-1.3
E_{ST} (CBS-Q)	-20.5	-14.1	-15.6	-6.5	--	--
E_{ST} (CCSD(T)/cc-pVTZ// CCSD/cc-pVDZ)	-16.5	-10.6	-15.4	-4.4	--	--

CONCLUSIONS

Compared with the phenyl oxenium ion **1** (Table 6), heteroaryl oxenium ions have reduced singlet−triplet gaps in favor of the triplet states. The 2- and 3-pyridinyl oxenium ions have only slightly reduced singlet−triplet gaps, but the 4-pyridinyl, pyrizidinyl, and pyrimidyl oxenium ions all have a computed ΔE_{ST} of less than −4 kcal/mol, opening up the possibility of reactivity from the triplet as well as rare open shell singlet states, sometimes seen in isoelectronic phenylnitrenes.

Table 6. Previously Computed Energies of the Lowest Irreducible Representations of the Phenyloxenium Ion **1**[1] irreducible representation ($\mathbf{C}_{2v}$) relative adiabatic energy (kcal/mol)

irreducible representation (C_{2v})	relative adiabatic energy (kcal/mol)
1^1A_1	0
1^1A_2	30.8
1^1B_1	48.3
1^1B_2	48.0
1^3A_2	22.1
1^3B_1	47.0
1^3B_2	29.9

We are currently working on developing photochemical precursors to these oxenium ions to study their reactivity; these computational studies will aid us in selecting the most interesting candidates for experimental study. These ions may be of fundamental interest as platforms for studying the relationship between electronic structure and reactivity for this important class of reactive intermediates.

REFERENCES

(1) Hanway, P. J.; Winter, A. H. *J. Am. Chem. Soc.* **2011**, *133*, 5086.

(2) Katsumata, S.; Lloyd, D. R. *Chemical Physics Letters* **1977**, *45*, 519.

(3) Dewar, M. J. S.; David, D. E. *J. Am. Chem. Soc.* **1980**, *102*, 7387.

(4) Geise, C. M.; Hadad, C. M. *J. Org. Chem.* **2000**, *65*, 8348.

(5) Cramer, C. J.; Dulles, F. J.; Falvey, D. E. *J. Am. Chem. Soc.* **1994**, *116*, 9787.

(6) Cramer, C. J.; Truhlar, D. G.; Falvey, D. E. *J. Am. Chem. Soc.* **1997**, *119*, 12338.

(7) Borden, W. T.; Gritsan, N. P.; Hadad, C. M.; Karney, W. L.; Kemnitz, C. R.; Platz, M. S. *Acc. Chem. Res.* **2000**, *33*, 765.

(8) Travers, M. J.; Cowles, D. C.; Clifford, E. P.; Ellison, G. B. *J. Am. Chem. Soc.* **1992**, *114*, 8699.

(9) McDonald, R. N.; Davidson, S. J. *J. Am. Chem. Soc.* **1993**, *115*, 10857.

(10) Widmark, P.-O.; Malmqvist, P.-Å.; Roos, B. O. *Theoretical Chemistry Accounts: Theory, Computation, and Modeling (Theoretica Chimica Acta)* **1990**, *77*, 291.

(11) Andersson, K.; Malmqvist, P.-Ö.; Roos, B. r. O. *Journal of Chemical Physics* **1992**, *96*, 1218.

(12) Aquilante, F.; De Vico, L.; Ferré, N.; Ghigo, G.; Malmqvist, P.-å.; Neogrády, P.; Pedersen, T. B.; Pitoňák, M.; Reiher, M.; Roos, B. O.; Serrano-Andrés, L.; Urban, M.; Veryazov, V.; Lindh, R. *Journal of Computational Chemistry* **2010**, *31*, 224.

(13) Karlstrom, G.; Lindh, R.; Malmqvist, P. A.; Roos, B. O.; Ryde, U.; Veryazov, V.; Widmark, P. O.; Cossi, M.; Schimmelpfennig, B.; Neogrady, P.; Seijo, L. *Comput. Mater. Sci.* **2003**, *28*, 222.

(14) Frisch, M. J.; et al. *Gaussian 09,* version A02; Gaussian, Inc.: Pittsburg, PA, 2009.

(15) Bendikov, M.; Duong, H. M.; Starkey, K.; Houk, K. N.; Carter, E. A.; Wudl, F. *J. Am. Chem. Soc.* **2004**, *126*, 7416.

(16) Kuzmanich, G.; SpaÃànig, F.; Tsai, C.-K.; Um, J. M.; Hoekstra, R. M.; Houk, K. N.; Guldi, D. M.; Garcia-Garibay, M. A. *J. Am. Chem. Soc.* **2011**, *133*, 2342.

(17) Perrin, C. L.; Rodgers, B. L.; O'Connor, J. M. *J. Am. Chem. Soc.* **2007**, *129*, 4795.

(18) Nagase, S.; Fueno, T. *Theoretical Chemistry Accounts: Theory, Computation, and Modeling (Theoretica Chimica Acta)* **1976**, *41*, 59.

CHAPTER 4: DIRECT SPECTROSCOPIC OBSERVATION OF CLOSED-SHELL SINGLET, OPEN-SHELL SINGLET, AND TRIPLET *P*-BIPHENYLYLOXENIUM ION

Taken in part from current manuscript.

INTRODUCTION

In spite of the importance of oxenium ions to such a diversity of chemists, oxenium ions are poorly understood. A problem that has hindered a better understanding of oxenium ions has been the lack of general methods to photogenerate these species that would allow them to be directly detected in order to study their reactivities, lifetimes, spectroscopic signatures, and electronic configurations. Studies of related intermediates (carbenes, nitrenes, nitrenium ions) have benefited tremendously from the ability to photogenerate these species from established precursors (azides, azirines, etc).[1-5] In contrast, there have been few good ways to generate oxenium ions photochemically. These ions have been suggested as intermediates from mixtures from multiphoton ionization studies and from mass spec ion fragmentations.[6-9] However the development of a robust single photon precursor to this species has proven to be difficult.

Some progress towards general photochemical precursors to oxenium ions has been made, and two discrete oxenium ions have recently been directly detected by laser flash photolysis (LFP).[10,11] In an important paper, Novak and Platz were the first to report the detection of an oxenium ion (the 4′-methyl-4-biphenylyloxenium ion), which was generated from the photolysis of the 4-(4-methylphenyl)-4-acetoxy cyclohexadienoyl derivative.[10] See Scheme 1. More recently, we observed the parent phenyloxenium ion as

a photoproduct of the phenyl hydroxylamine tetrafluoroborate salt.[11] In addition to a concomitant homolytic process, this hydroxylamine salt undergoes heterolytic scission of the O-N bond to lead to the formation of the singlet phenyloxenium ion and neutral ammonia.[11] Both the detected oxenium ions were seen in their singlet ground states.

The possible use of protonated hydroxylamines as photoprecursors to oxenium ions is an intriguing one. These photoprecursors offer a few advantages. First, they are easy to prepare synthetically. Second, they are positively charged rather than neutral and eject a neutral leaving group (ammonia). In principle, a positively charged precursor allows the photolysis to generate oxenium ions in solvents that are non-ionizing. In contrast, uncharged precursors require ionizing solvents because they generate an ion pair starting from a neutral species. Finally, they are not, in principle, restricted to generating certain oxenium ion structures.

To test the scope of this photoprecursor, we synthesized the 4-biphenyl-hydroxylamine hydrochloride salt, which we anticipated could lead to the 4-biphenylyloxenium ion and allow comparisons to the neutral photoprecursor studied by Novak and Platz.[10] We are pleased to report a combined femtosecond transient absorption (fs-TA), nanosecond transient absorption (ns-TA) and nanosecond time-resolved resonance Raman (ns-TR^3) spectroscopic investigation of the photophysics and photochemistry of compound 1 to directly observe the formation of the open-shell singlet *p*-biphenyloxeniumion, the closed-shell singlet state *p*-biphenyloxeniumion, the triplet state *p*-biphenyloxeniumion, and *p*-biphenyloxy radical intermediates after ultraviolet photo-excitation in MeCN solution. To our knowledge this is the first direct detection of an open-shell singlet or a triplet state of an oxenium ion in solution using LFP.

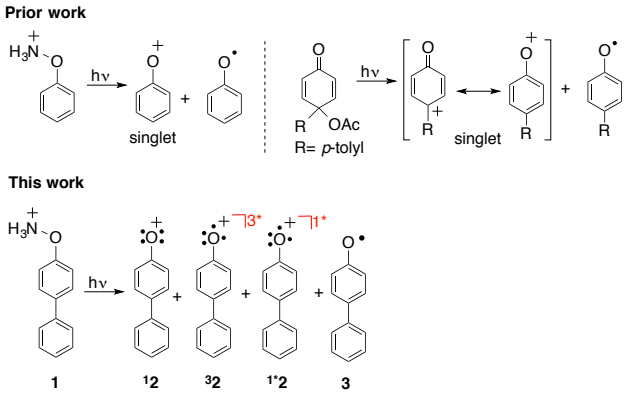

Scheme 1. The two prior studies that have detected discrete oxenium ions by LFP,[10,11] and an overview of this work.

Experimental and Computational Methods

The precursor sample compound for the photochemistry and time-resolved spectroscopy experiments was synthesized from a modification of a known procedure of aryloxyamines in 2001.[12,27] See Supporting Information for synthetic procedures. Spectroscopic grade acetonitrile (MeCN) was used to prepare sample solutions for use in the time-resolved spectroscopy experiments.

A. Femtosecond Transient Absorption (fs-TA) Experiment. Fs-TA measurements were done using a femtosecond regenerative amplified Ti:sapphire laser system in which the amplifier was seeded with the 120 fs laser pulses from an oscillator laser system. The laser probe pulse was produced by utilizing ~5% of the amplified 800 nm laser pulses to generate a white-light continuum (350-800 nm) in a CaF_2 crystal and then this probe beam was split into two parts before traversing the sample. One probe laser beam goes through the sample while the other probe laser beam goes to the reference spectrometer in order to monitor the fluctuations in the probe beam intensity. For the experiments discussed in this work, a 10 ml solution was flowed through a 2 mm path-length cuvette. This flowing sample was then excited by a 267 nm pump laser beam. An absorbance of 1

at 267 nm was used for the sample solutions for the fs-TA experiments in order to maintain the same number of photons being absorbed for the same irradiating conditions for the samples.[28,29]

B. Nanosecond Transient Absorption (ns-TA) Experiment. The ns-TA experiments: Nanosecond time-resolved transient absorption (ns-TA) measurements were carried out with a LP920 laser flash spectrometer provided by Edinburgh Instruments Ltd. The probe light source is a 450 W ozone free Xe arc lamp with 10 Hz to single shot operation versatile sample chamber with integral controller, high speed pump and probe port shutters, sample holder, filter holders, which produces a continuous spectrum between 150 to 2600 nm. Measurements of the ns-TA spectra were performed according to the following procedure. The fresh sample solutions were excited by a Q-switched Nd:YAG laser (4^{th} harmonic line at λ=266 nm). The probe light from a pulsed xenon arc lamp was passed through various optical elements, samples, and a monochromator before being detected by a fast photomultiplier tube and recorded with a TDS 3012C digital signal analyzer. In the kinetics mode, a photomultiplier detector or InGaAs PIN detector is used and the transient signal acquired using a fast, high resolution oscilloscope. In the spectral mode an array detector is fitted to the spectrograph exit port to measure a full range of wavelengths simultaneously. Unless specified otherwise, the ns-TA experiments were performed in air saturated solutions and the sample solutions were made up to have an absorbance of 1 at 266 nm.

C. Nanosecond Time-Resolved Resonance Raman (ns-TR^3) Experiments. The ns-TR^3 experiments were done employing an experimental setup and methods detailed previously[29] and only a brief account is provided here. The fourth harmonic of a Nd:YAG

nanosecond pulsed laser supplied the 266 nm pump wavelength and the 341.5 nm probe wavelength came from the second Stokes hydrogen Raman-shifted laser line produced from the fourth harmonic of a second Nd:YAG laser). The pump pulse photo-excited the sample to start the photochemical processes and the probe pulse monitored the sample and the intermediate species formed. The laser beams were lightly focused and lined up so that they merged together onto a flowing sample. A pulse delay generator was utilized to electronically set the time delay between the pump and probe laser pulses. The Raman scattered signal was collected using a backscattering geometry and observed by a liquid nitrogen-cooled charge-coupled device (CCD) detector. The ns-TR^3 spectra shown here were found from subtraction of an appropriately scaled probe-before-pump spectrum from the correlated pump-probe resonance Raman spectrum to mostly get rid of non-transient bands. The Raman bands of MeCN were used to calibrate the Raman shifts with an estimated uncertainty of 5 cm^{-1}. The sample concentrations in ns-TR^3 were ~5×10^{-4} M.

D. Product Studies. Photolysis studies were performed by the addition of 5 mg 4-biphenylyl hydroxylamine hydrochloride **1** to 3 mL of solvent. This solution was then degassed and photolyzed for 1 hr in a Rayonet photoreactor. In the case the reaction was not complete, the sample was afterwards photolyzed to completion. Thermolysis studies were performed by refluxing 10 mg of the precursor compound **1** in 6 mL solvent for 1 hr after degassing the solution.

E. Density Functional Theory (DFT) Calculations. DFT calculations were performed employing the (U)B3LYP method with a 6-311G(d,p) basis set. The Raman spectra were found from computing the Raman intensities from transition polarizabilities computed by numerical differentiation, with an assumed zero excitation frequency. A Lorentzian

function with a 15 cm^{-1} bandwidth for the vibrational frequencies and a frequency scaling factor of 0.974 was used in the comparison of the calculated results with the experimental spectra.[30] TD-DFT was used to calculate the excitation energies and oscillator strengths, the simulation of UV-vis spectra of selected intermediates and excited state were obtained from (U)B3LYP DFT calculations employing a 6-311G(2d,p) basis set in PCM solvent mode. No imaginary frequency modes were observed at the stationary states of the optimized structures. All of the calculations were done using the Gaussian 09 program suite.[13]

RESULTS AND DISCUSSION

1. Femtosecond and nanosecond laser flash photolysis (LFP) investigation of p-biphenylylhydroxylamine hydrochloride 1.

Figure 1 shows the evolution of the transient absorption of the photoprecursor in acetonitrile from 2 ps to 3022 ps. Immediately after the laser pulse, a broad transient absorption with maxima at 350, 394, and 630 nm emerges. This transient can be assigned to the first excited singlet state (S_1) of the photoprecursor after 267 nm excitation, which grows in with a time constant of 350 fs. As the maximum absorption at around 630 nm and the shoulder absorption at around 394 nm quickly drop off, a sharp absorption at lower wavelength grows in and undergoes a hypsochromic shift from 350 nm to 345 nm. After 200 ps, the transient absorption at 345 nm and 382 nm reaches a plateau until 3000 ps. This 345 nm transient can still be seen in the nanosecond transient absorption experiments and decays over ~ 39 μs. This transient can be definitively assigned to the *p*-biphenyloxy radical as seen by ns-TR^3 experiments (described below). However, the transient absorption at 630 nm still decays by a slow process compared to the fast decay

process before 200 ps. In addition, a shoulder peak appears at 560 nm which is accompanied by the fast decay of 630 nm.

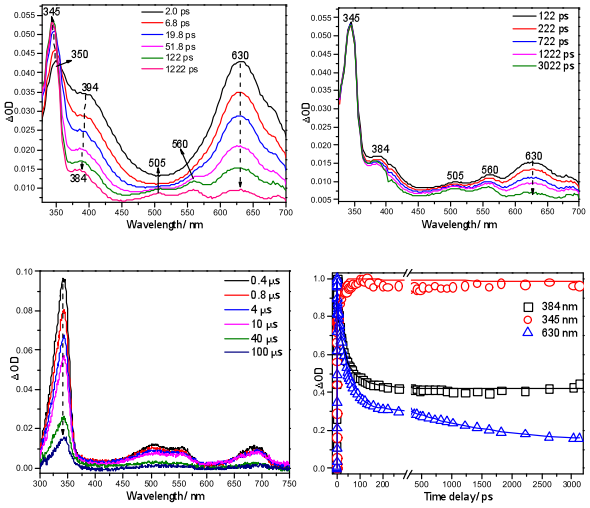

Figure 1. The TA spectra of species produced in MeCN acquired after 266 nm irradiation of the precursor compound 1 (Top left) LFP from 2 ps to 122 ps; (Top right) from 122 ps to 3022 ps); (Bottom left) nanosecond-TA spectra from 0.4 ms to 100 ms. Bottom right are the kinetics of the characteristic fs-TA absorption bands observed at 345 nm, 380 nm and 630 nm for the fs-TA spectra observed after 266 nm photoexcitation of 1 in MeCN. See text for more details.

The fast disappearance of the 630 nm and 390 nm bands, which can be attributed to S_1 of the photoprecursor, is associated with the appearance of several new transient species. In addition to the radical absorption at a low wavelength described above, two additional transient species are seen. One intermediate, also absorbing at 630 nm, decays over ~42 ps. A second transient, observed as a peak at ~394 nm, decays over ~48.8 ps. Based on TD-DFT computations of the UV-Vis spectra and trapping studies, we assign the transient absorbing at 630 nm (t = 42 ps) to the triplet oxenium ion, the transient absorbing at ~394 nm (t = 49 ps) to the open-shell singlet excited state oxenium ion (described below). After 122 ps, the 394 nm transient absorption undergoes a hypsochromic shift from 394 nm to 384 nm. The transient of 384 nm decays so little

over 3000 ps that it is difficult to obtain a good kinetic fit, but approximate fits give a time constant of ~5 ns. In contrast to the radical absorption, which we observe in the nanosecond LFP experiments, this transient is not detected in the nanosecond LFP experiments. Thus, the lifetime of this final transient must be between 3-20 ns (our "temporal"blindspot"between the femtosecond and nanosecond LFP setups). We assign this transient absorbing between ~384 nm (t ~ 5 ns) to the ground-state closed-shell singlet oxenium ion (described below).

In an attempt to convincingly confirm how many species involved after excitation of the photoprecusor **1**, the principal components via SVD method was used to analyze the data obtained at the beginning of 150 ps.

The principal components analysis found that there are four components accounting for the evolution spectra at early delay time. Figure 2 displays the principal spectra and kinetics of the first excited singlet state (S_1) of the photoprecursor ($^{1*}1$), triplet oxenium ion ($^{3}2$), open-shell singlet oxenium ion ($^{1*}2$) and *p*-biphenyloxy radical (3).

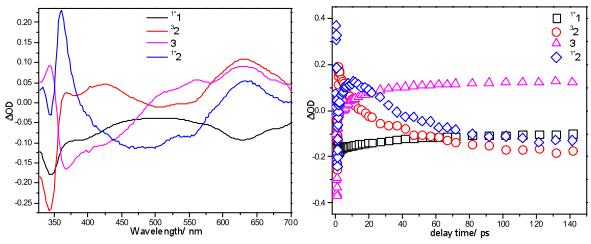

Figure 2. The principal spectra (right) and kinetics (left) of four components obtained by principal components via SVD at the beginning of 150 ps.

For the transient absorption at 505 and 560 nm, these two bands correspond to different species which is evident by inspecting the transients at 560 nm and 505 nm. At 3022 ps these bands are the same height even though the band at 560 nm started with a larger absorption at 122 ps. The 505 nm transient absorption is also observed in ns-TA

experiments and this band can be assigned to the *p*-biphenyloxy radical (described below). The bands at later delay times at 560 and 630 nm decay over ~1200 ps and ~1600 ps respectively. Those two bands are possibly associated with the intermediates formed by the reaction of the triplet oxenium ion with ammonium, chloride ion or a proton.

2. Lifetimes for the observed transients.

In order to obtain the time constant of the different intermediates, a sum of convoluted exponentials function was used to fit a kinetic trace at the selected wavelength. Where t_p is instrument response time, t_0 is time zero, A_i and t_i are amplitudes and decay times respectively. The fitting curve and the residuals are listed in the Supporting Information. Table 1 displays the time constants and amplitudes of the fitting for the selected wavelength.

$$S(t) = e^{-(\frac{t-t_0}{t_p})^2} * \sum_i A_i e^{-\frac{t-t_0}{t_i}}$$

Table 1. Shown are the time constants determined from the fitting for the selected wavelength.

Wavelength, nm	τ_1, ps	τ_2, ps	τ_3, ps
345	14		
384	4	49	
630	2	42	1613

As mentioned above, the 345 nm transient absorption was assigned to the *p*-biphenyloxy radical, the fitting done for 345 nm found a growth time constant (14 ps) of the *p*-biphenyloxy radical. The *p*-biphenyloxy radical can survive for a long time in acetonitrile (see Figure 1 bottom left). A biexponential function was used to fit the kinetics of 345 nm obtained from the ns-TA spectra and found that a 39 μs time constant could be obtained, which is the lifetime of the *p*-biphenyloxy radical. In contrast, the kinetics of 384 nm could be fitted by a biexponential function and two time constants can be obtained. The 4

ps is the growth time constant for the generation of the open-shell singlet oxenium ion, while the 49 ps is associated with the internal conversion (IC) process from the open-shell singlet oxenium ion to the closed-shell singlet oxenium ion. Whereas for the kinetics of 630 nm, a triexponential function was required to obtain a best-fit at this wavelength. The 2 ps time constant accounts for the generation of the triplet oxenium ion and the 42 ps time constant is the lifetime of this triplet oxenium ion and the 1.6 ns time constant results from the decay of the intermediate produced from the triplet oxenium ion reacting with the proton, ammonium or chloride ion.

3. ns-TR^3 experiments identify the long-lived transient as the radical.

In the ns-TA spectra a longer-lived transient species has a strong band at 345 nm accompanied by a smaller band at 505 nm (see Figure 1). To learn more about the nature of this longer lived species, we obtained ns-TR^3 spectra of it using a 341.5 nm probe wavelength and this is shown in Figure 3. Time-dependent density functional theory (TD-DFT) computations were done to estimate the transient absorption spectrum for the *p*-biphenyloxy radical and the comparison between calculated spectrum and experimental spectra is shown in Figure 4 and this suggests that the strong 345 nm long lived band with its weaker 505 nm band may be due to the *p*-biphenyloxy radical. DFT calculations were also done to estimate the normal Raman spectrum of the *p*-biphenyloxy radical and this spectrum is shown at the bottom of Figure 3 and compared to the ns-TR^3 spectrum obtained using a 341.5 nm probe wavelength at 50 ns after 266 nm photo-excitation of **1** in MeCN that is shown at the top of Figure 3. Inspection of Figure 3 shows that there is excellent agreement between the vibrational frequency patterns of the calculated normal Raman spectrum and the ns-TR^3 spectrum obtained at 50 ns. The dotted lines indicate the

correspondence of the vibrational features in the calculated and experimental spectra in Figure 3. The preceding results displayed in Figures 3 and 4 lead us to assign the relatively long lived intermediate with a strong peak at 345 nm and a smaller band at 505 nm to the *p*-biphenyloxy radical species. The ns-TA spectra shown in Figure 1 had their kinetic fit and this data is shown in Supporting information along with a best fit of a biexponential function that gave decay time constants of t_1= 39 ms and t_2= 258 ms. The first decay time constant is attributed to the decay of the p-biphenyloxy radical to form another species that does not absorb strongly at 345 nm. The second decay time constant is not yet clear but may be due to some reaction of the radical to form a species that absorbs very little at 345 nm.

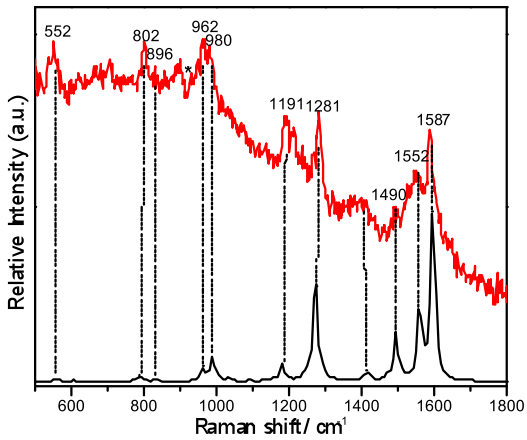

Figure 3. (Top) Ns-TR[3] spectrum obtained at 50 ns after 266 nm photo-excitation of 1 and using a 341.5 nm probe wavelength in MeCN. Asterisks represent solvent subtraction artifacts. (Bottom) Shown is the calculated normal Raman spectrum of the *p*-biphenyloxy radical (see text for more details).

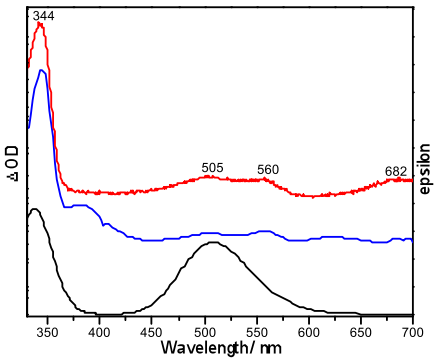

Figure 4. Comparison of the experimental transient absorption spectrum obtained at 400 ns (top), to that obtained at 3022 ps (middle) with that computed for the UV spectrum (TD-B3LYP/6-311+G(2d,p)) of the *p*-biphenylyl radical (bottom).

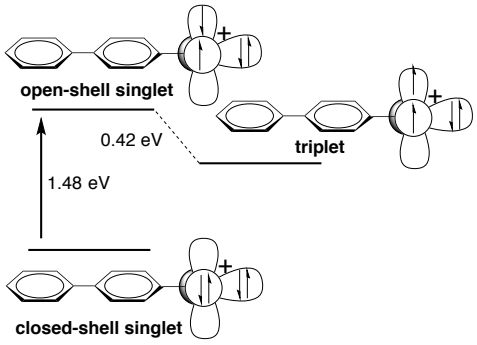

Figure 5. Shown is the TD-DFT calculated relative energies of the closed-shell singlet *p*-biphenylyloxenium ion (S_0), the excited open-shell singlet *p*-biphenylyloxenium ion (S_1) and the triplet *p*-biphenylyloxenium ion (T_1).

4. Assignment of the other bands by time-dependent density functional theory (TD-DFT) computations.

To help assign the remaining transients, we have performed TD-DFT calculations to estimate the absorption bands for some likely intermediate species that could be generated from the decay of the excited singlet state of 1. TD-DFT computations have been previously shown to be useful in estimating absorption bands provided the ground state can predominantly be described by a single-reference wavefunction. For example, they are frequently used for assigning absorption bands for carbenes and nitrenes.[31-33]

It is important to consider that oxenium ions can adopt different electronic states.[34,35] Our computations (Figure 5) indicate that the *p*-biphenylyloxenium ion has a closed-shell singlet ground state with a gap to the lowest energy triplet state of ca. 23 kcal/mol and a vertical gap to the open-shell singlet state of 34 kcal/mol. Thus, unlike many carbenes, it is not possible to see equilibration of singlet and triplet states.

Figure 6 (right) displays the comparison of the fs-TA spectrum obtained at a time-delay of 6.8 ps (black line) with the absorption spectra calculated at the (TD-B3LYP/6-311+G(2d,p)) level of theory for the open-shell singlet *p*-biphenylyloxenium ion (blue line) and the triplet *p*-biphenylyloxenium ion (red line). The computed absorption spectrum of the triplet *p*-biphenylyloxenium ion has two bands located at 342 nm and 621 nm that correspond to the experimentally observed transient absorption bands at 345 nm and 630 nm. The calculated absorption spectrum of the open-shell singlet *p*-biphenylyloxenium ion has a band located at 384 nm that corresponds with the experimentally observed transient absorption band located at 394 nm. These comparisons suggest that both the open-shell singlet and triplet *p*-biphenylyloxenium ion ions are observed in the fs-TA experiments following 266 nm photo-excitation of 1 in MeCN.

The carrier of the final band at 384 nm is less readily assignable. This transient follows the open-shell singlet *p*-biphenylyloxenium ion and has a time constant of 5-20 ns, but is not the open-shell singlet oxenium ion, the triplet oxenium ion, or the radical. Given that all alternative assignments are less plausible, we tentatively assign it to the closed-shell singlet ground state of the oxenium ion. That means that the open-shell singlet *p*-biphenylyloxenium ion will undergo an IC process to form the closed-shell singlet *p*-biphenylyloxenium ion. Figure 6 (left) presents the comparison of the fs-TA

spectrum obtained at a time-delay of 1222 ps (black line) with the absorption spectra calculated for the closed-shell singlet *p*-biphenylyloxenium ion. This further implies that the 384 nm transient absorption is associated with the closed-shell singlet *p*-biphenylyloxenium ion. TD-DFT computations described below indicate the singlet excited state is ~35 kcal/mol higher in energy than the closed-shell singlet, close to what a recent computational study (CASPT2) found for the energy gap between the open-shell singlet state of phenyloxenium ion and the closed shell configuration (31 kcal/mol).[14] Given that photolysis is performed at 267 nm, each photon carries 107 kcal/mol of radiant energy and it is certainly energetically plausible that an excited state of ~35 kcal/mol higher in energy than the ground state of the oxenium could be formed, considering that an O-N bond enthalpy is ~38 kcal/mol. Photogeneration of a reactive intermediate excited state is unusual but not without precedent. For example, Platz detected the simultaneous generation of the open-shell singlet and closed-shell singlet fluorenyl carbene upon photolysis of the diazo precursor.[36] Additionally, alternative assignments are less plausible. It is at least in principle possible to observe an S_2 to S_1 conversion of the excited state of **1**, but the carrier of the transient is too long-lived for this possibility to be seriously considered. A more plausible alternative assignment is as an excited T_1 triplet state of the oxenium ion (e.g. a p,p* triplet oxenium ion), but we view this alternative as less likely given that our computations indicate that the triplet excited state of the photoprecursor is a transition state for forming the n,p* triplet oxenium ion.

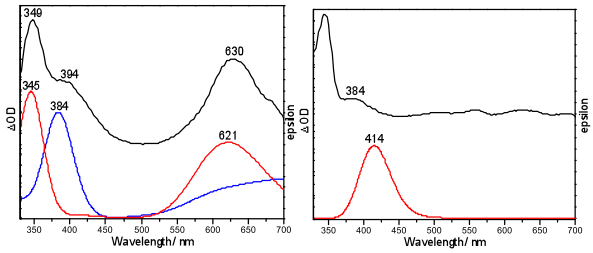

Figure 6. (Right) Comparison of fs-TA experimental spectrum at 6.8 ps with the computed UV spectra (TD-B3LYP/6-311+G(2d,p)) of the excited open-shell singlet *p*-biphenylyloxenium ion (blue) and the triplet *p*-biphenylyloxenium ion (red); (Left) Comparison of fs-TA experimental spectrum at 1222 ps and computed UV spectra (TD-B3LYP/6-311+G(2d,p)) of the closed-shell singlet ground state of *p*-biphenylyloxenium ion.

5. Product studies from photolysis and thermolysis of 1.

We also hoped to gain insight into the intermediates resulting from the precursor **1** via product studies from thermolysis and photolysis. Table 1 shows the products formed via photolysis and thermolysis under different conditions.

Photolysis in water or acetonitrile gives almost exclusively the reduction product, *p*-biphenylol, with only trace amounts of a chloro trapping adduct. When chloride is added as a trap in water, however, the major product is the chloro adduct, with the reduced product being the minor product. It is possible to envision mechanisms to the reduced product via all the observed intermediates in the photolysis. The radical could form the reduced product via an H-atom abstraction, while the oxenium ions could form the reduction product either via a hydride abstraction or via two H-atom abstractions followed by a deprotonation. The chloride trapping adduct is clear evidence for an oxenium ion intermediate, as oxenium ions are known to be trapped by nucleophiles at the *ortho* and *para* positions of the ring.[24,25,37]

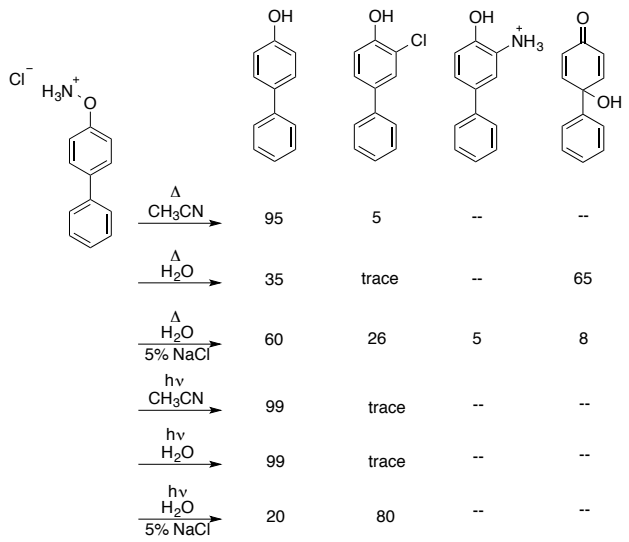

Table 1. Product studies from the photolysis of compound **1**. Percentages are based on relative ^{1}H NMR integration.

Product studies from thermolysis are similar to those obtained by photolysis. Thermolysis in acetonitrile gives principally the reduced product as seen in the photolysis in acetonitrile. In water, however, the major product is a water trapping adduct at the *para* position to form a dearomatized product. When the thermolysis is performed in water with added Cl^- as a trap, a complex mixture of the reduced product, the ammonium adduct, the chloro adduct, and the water adduct are obtained. A plausible explanation of why water adds to the *para* position to generate the dearomatized product while chloride and ammonia add to the *ortho* position could be that *para* addition is kinetically favored, but reversible. Eventually the aromatized thermodynamic *ortho* adduct is formed. However, once water adds, a fast deprotonation of the water addition product could render this step irreversible and trap it as the dearomatized product.

Discussion and photochemical reaction scheme.

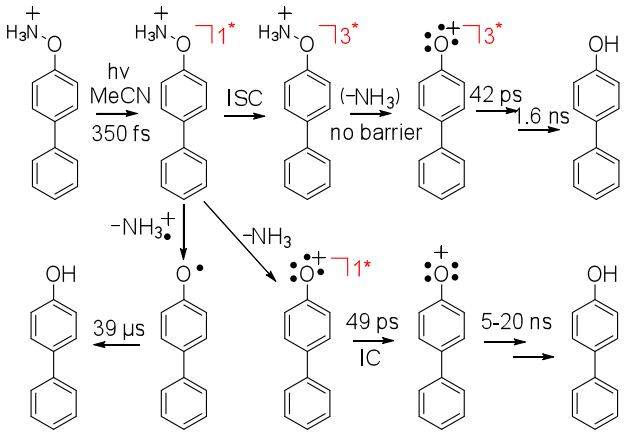

Scheme 2. Probable reaction pathways and time constants for the open-shell singlet *p*-biphenylyloxenium ion, the ground state of the singlet *p*-biphenylyloxenium ion, the triplet state *p*-biphenylyloxenium ion and *p*-biphenyloxy radical are shown. Note that the triplet excited state of the photoprecursor is computed to be a transition state for a barrierless dissociation of ammonia to give the triplet oxenium ion.

Based on the data presented above, the proposed photochemical reaction pathways are shown in Scheme 2. Within 350 fs, the first excited singlet state is formed of 1, which partitions into three transients: the *p*-biphenyloxy radical, the open-shell singlet *p*-biphenylyloxenium ion and the triplet *p*-biphenylyloxenium ion. The excited singlet *p*-biphenylyloxenium ion (S_1) state may decay via intersystem crossing (ISC) to the triplet *p*-biphenylyloxeniumion (T_1) species, or via internal conversion (IC) to the ground state of singlet *p*-biphenylyloxenium ion (S_0). Internal conversion is probably more likely than ISC since in this case ISC is spin-orbit coupling forbidden since the change in spin angular momentum is not compensated by a change in orbital angular momentum and would thus be expected to be slow. In any event, all of the transient species lead to formation of the reduced product, p-biphenylol in the absence of an added trap. The ISC of the photoprecursor to form the triplet state is not entirely unexpected since biphenyl itself has a quantum yield of intersystem crossing (F_{ISC}) of 0.85.[38] Remarkably, in sharp

contrast to carbenes and nitrenes, the triplet state of the oxenium ion is shorter-lived than the closed-shell singlet state. For carbenes and nitrenes, usually only the triplet states can be seen with nanosecond spectroscopy and the singlets have lifetimes on the order of tens of picoseconds. Possibly the shorter-lived triplet is due to the fact that singlet carbenes/nitrenes have a facile C-H insertion pathway and often decay via ISC to lower-energy triplet states. Here, C-H insertion is apparently not an observable reaction channel for singlet oxenium ions, and the triplet is the higher-energy species, making ISC not a favorable decay channel.

CONCLUSIONS

Using fs-TA, ns-TA and ns-TR^3 spectroscopic techniques as well as DFT calculations, the present contribution reports an investigation of the photophysical and photochemical reactions of 1 to produce the open-shell singlet *p*-biphenylyloxenium ion, the triplet state *p*-biphenylyloxenium ion and *p*-biphenyloxy radical intermediates. The properties and kinetics of these intriguing reactive intermediates are discussed. This study provides an intriguing demonstration of the importance of excited state dynamics in governing electronic state population of photoprecursors, since the system of Novak and Platz leads to a related closed-shell singlet oxenium ion, whereas the protonated hydroxylamine discussed in this paper leads to the radical, the open-shell singlet and closed-shell singlet states of the oxenium ion and the triplet state of the oxenium ion. To our knowledge, this is the first detection and characterization of a short-lived photochemically generated open-shell singlet or triplet phenyloxenium ion.

Synthesis of *N*-4-phenylphenoxyphthalimide. Based on a published synthesis[12]. 326 mg (2mmol, 1eq) of N-hydroxyphthalimide, 200 mg (2mmol, 1equiv) of CuCl, 792 mg

(4 mmol, 2 equiv) of phenylboronic acid, and ~500 mg of 4Å molecular sieves were added to a round bottom flask. 15 mL of 1,2-dichloroethane followed by 180 μL (2.2 mmol, 1.1 equiv) of pyridine were added to the flask. The reaction was stirred for 72 hours under air at ambient temperature. The reaction was monitored by TLC (75:25 Hexanes:Ethyl Acetate). The reaction was allowed to react for 72 hours and then the solvent was evaporated under reduced pressure. The product was separated by column chromatography (7:3 Hexanes:Ethyl Acetate). A white solid (N-biphenoxyphthalimide) was collected and dried by high vacuum, to give 92.6% yield (480.8 mg), of the desired product. This product was then used for the next step in the synthesis.

^{1}H NMR of above *N*-4-phenylphenoxyphthalimide

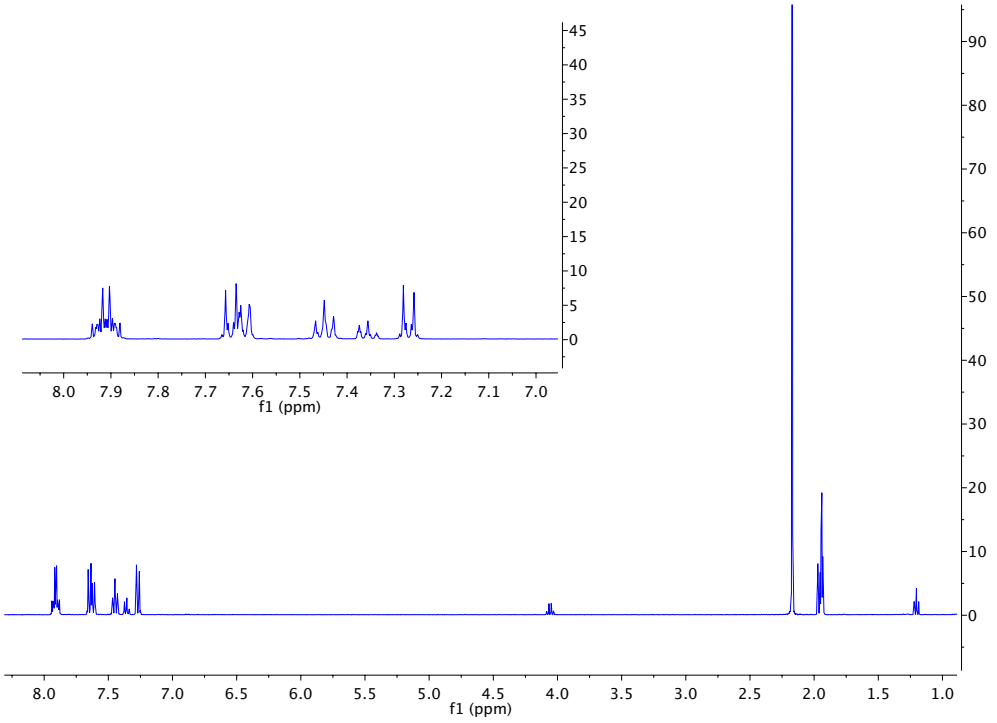

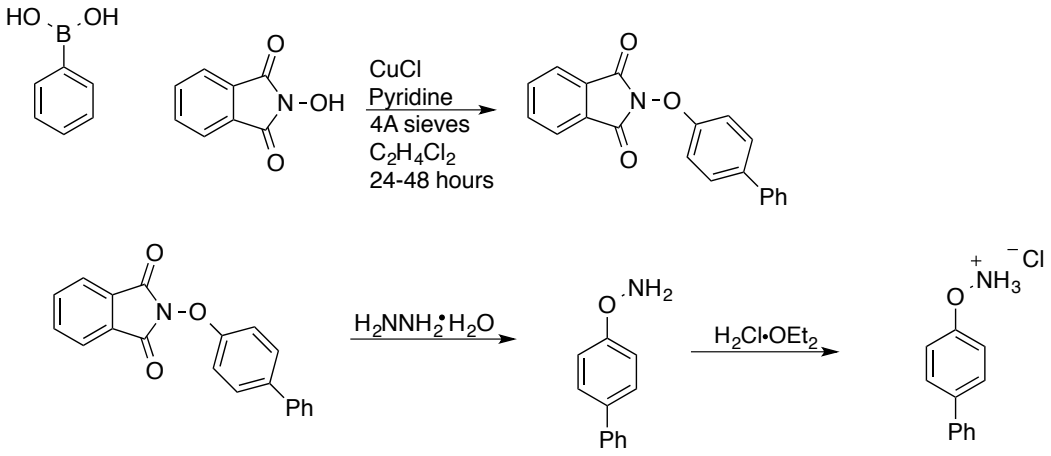

Figure 7. Synthesis of compound **1.**

Synthesis of 4-biphenylhydroxylamine hydrochloride 3. 480.8 mg (1.52 mmol, 1 equiv) of N-phenoxyphthalamide was added to a flask containing 100 mL of 10% MeOH in $CHCl_3$ and 0.74 mL (15.2 mmol, 10 equiv) of hydrazine monohydrate. A colorless solution was formed, which yielded a white precipitate over time. The reaction was monitored by TLC (75:25 Hexanes:Ethyl Acetate) and allowed to react overnight (12 hours). The filtered solid was then purified by column chromatography (75:25 Hexanes:Ethyl Acetate). The resulting product was dissolved in ether, to which $HCl*OEt_2$ (ca. 0.4 mL) was added until the TLC spot no longer moved. This signified the protonation of the hydroxylamine to the hydroxylamine hydrochloride salt. This solution was then dried under reduced pressure to yield 222 mg of the desired salt. (222 mg, 65.7% yield). The product was reasonably stable stored in a freezer in the dark

^{1}H NMR of above 4-biphenyl hydroxylamine hydrochloride

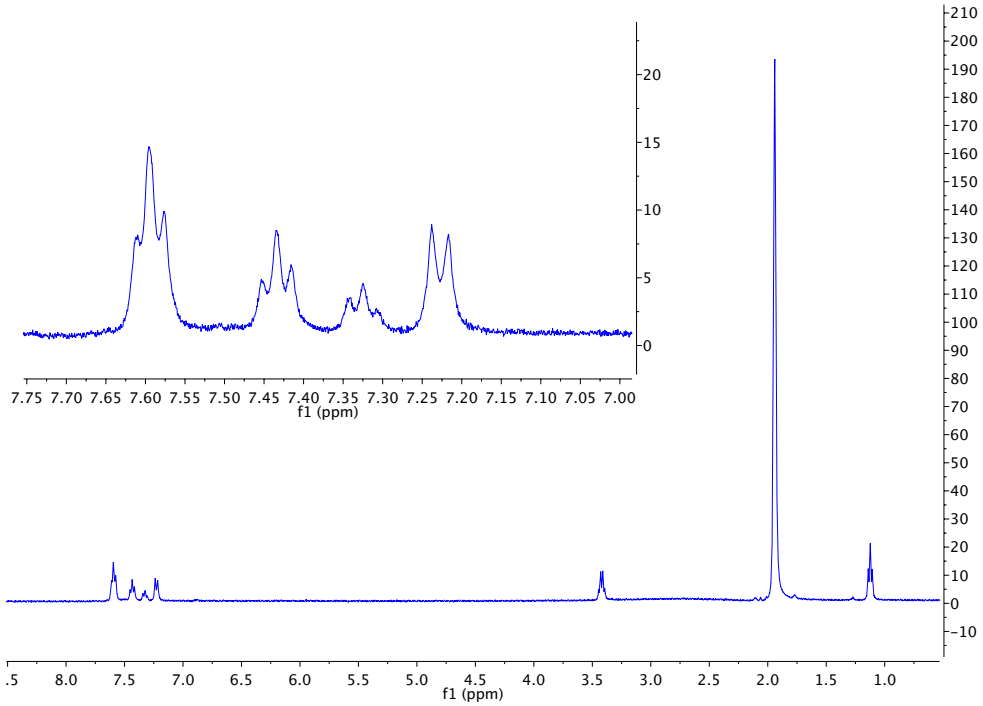

REFERENCES

(1) Zhang, Y.; Burdzinski, G.; Kubicki, J.; Platz, M. S. *J. Am. Chem. Soc.* **2008**, *130*, 16134.

(2) Wang, J.; Burdzinski, G.; Kubicki, J.; Platz, M. S. *J. Am. Chem. Soc.* **2008**, *130*, 11195.

(3) Winter, A. H.; Gibson, H. H.; Falvey, D. E. *J. Org. Chem.* **2007**, *72*, 8186.

(4) Winter, A. H.; Thomas, S. I.; Kung, A. C.; Falvey, D. E. *Organic Letters* **2004**, *6*, 4671.

(5) Platz, M. S. *Acc. Chem. Res.* **1995**, *28*, 487.

(6) Siuzdak, G.; North, S.; BelBruno, J. J. *J. Phys. Chem.* **1991**, *95*, 5186.

(7) Hwang, W. G.; Kim, M. S.; Choe, J. C. *J. Phys. Chem.* **1996**, *100*, 9227.

(8) Kosmidis, C.; Ledingham, K. W. D.; Kilic, H. S.; McCanny, T.; Singhal, R. P.; Langley, A. J.; Shaikh, W. *The Journal of Physical Chemistry A* **1997**, *101*, 2264.

(9) Syage, J. A.; Steadman, J. *J. Phys. Chem.* **1992**, *96*, 9606.

(10) Wang, Y. T.; Wang, J.; Platz, M. S.; Novak, M. *J. Am. Chem. Soc.* **2007**, *129*, 14566.

(11) Hanway, P. J.; Xue, J.; Bhattacharjee, U.; Milot, M. J.; Ruixue, Z.; Phillips, D. L.; Winter, A. H. *J. Am. Chem. Soc.* **2013**, *135*, 9078.

(12) Petrassi, H. M.; Sharpless, K. B.; Kelly, J. W. *Organic Letters* **2000**, *3*, 139.

(13) Frisch, M. J.; et al. *Gaussian 09,* version A02; Gaussian, Inc.: Pittsburg, PA, 2009.

(14) Hanway, P. J.; Winter, A. H. *J. Am. Chem. Soc.* **2011**, *133*, 5086.

CHAPTER 5
META-DIMETHYLAMINO PHENYLOXENIUM ION: STUDIES ON A GROUND-STATE TRIPLET ION

INTRODUCTION

Recently ground state singlet oxenium ions have been observed directly.[1,2] Along with these studies, computational studies have shown how we can manipulate the singlet triplet gap for aryl oxenium ions.[3] This ability to control the singlet triplet gap allows for the potential to observe the reactivity of oxenium ions as either a singlet or triplet ground state. This computational study suggested that electron donating groups on the meta position of an aryloxenium ion ring leads to a relative stabilization of the triplet state compared to the singlet state.

Computational studies indicate m-dimethylamino phenyloxenium ion is a ground-state triplet

In order to investigate the reactivity and nature of ground-state triplet oxenium ions, we proposed using the m-dimethylamino phenyloxenium ion precursor **1** shown in Figure 1. The m-dimethylamino phenyloxenium ion is computed to have a triplet ground state by 12 kcal/mol (B3LYP/cc-pVTZ). In a similar study the m-amino phenyloxenium ion was computed (B3LYP/cc-PVTZ) to have a ΔE_{ST} of 4.9 kcal/mol by DFT methods[4] as opposed to a ΔE_{ST} of -1.0 kcal/mol by the high level multireference CASPT2/pVTZ level of theory.[3] This error of ~6 kcal/mol allows for a strong possibility for the m-dimethylamino phenyloxenium ion to be a triplet ground state. Thus, the m-dimethylamino phenylhydroxylamine hydrochloride salt **1** was synthesized for studies.

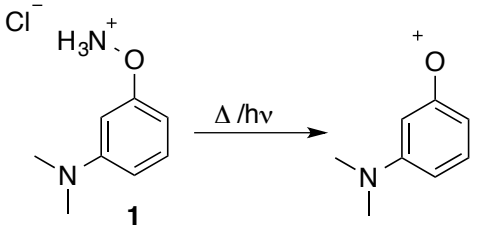

Figure 1: Proposed scheme for the formation of the m-dimethylamino phenyloxenium ion from precursor **1**.

Product studies from photolysis and thermolysis of m-dimethylamino phenylhydroxylamine hydrochloride indicate a m-dimethylamino phenyloxenium ion intermediate.

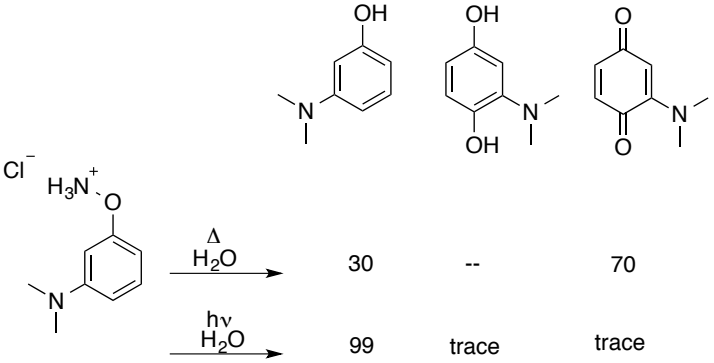

Table 1: Product study analysis obtained from LCMS and ^{1}H NMR.

Product studies have been obtained in water through the thermolysis and photolysis of precursor **1**. Thermolysis studies (Table 1) form primarily form a m-dimethylamino quinone as the major product with m-dimethylamino phenol as the minor product. The formation of the dimethylamino quinone provides strong evidence for the formation of the m-dimethylamino phenyloxenium ion intermediate since this product is expected from water trapping an oxenium ion intermediate electrophile.[1] The photolysis studies form primarily the m-dimethylamino phenol along with trace amounts of other products shown in Table 1. The photolysis leading only to the m-dimethylamino phenol structure is somewhat misleading since other products are formed during the photolysis, but these structures appear to absorb as well secondary photoreactions occur. Dimers

appear to form and eventually these too lead to the formation of only phenol. This higher ratio of products suggesting oxenium ion intermediates in thermolysis studies compared to photolysis studies has been observed in previous work as well.[1]

Matrix isolation EPR studies indicate a triplet ground state

Since it is expected that the ground state of the m-dimethylamino phenyloxenium ion is a ground state triplet, EPR studies were performed in order to see if we could observe the triplet m-dimethylamino phenyloxenium ion. For these studies, precursor **1** was dissolved in ethanol and cooled to 4 K. Photolysis of this sample was then performed with a mercury arc lamp. The EPR spectrum obtained from this study is shown in Figure 2.

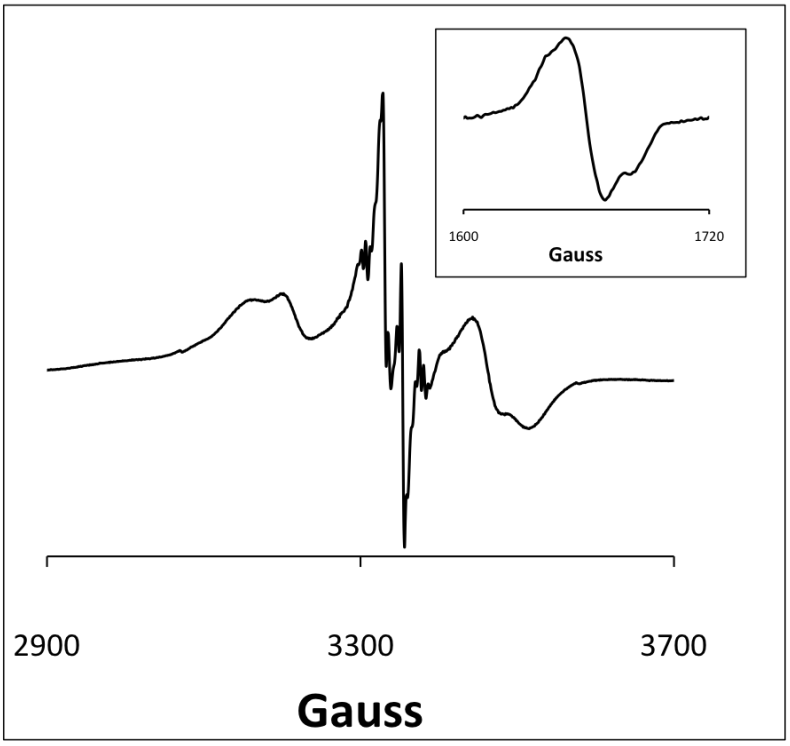

Figure 2. EPR of photolysis of compound **1** in ethanol at 4 K.

First, there is a large absorption centered around 3300 gauss. The sharp central peaks are likely organic radical impurities, with an organic radical spectrum

superimposed on top. The large splitting observed is from the zero field splitting from the m-dimethylamino phenyloxenium ion. The peak at 1650 gauss shown in the subset of Figure 2, is strong evidence of the half field splitting of a triplet species. Given that there is essentially no chance for thermal population of an excited state at 4K, these studies are suggestive of a ground state triplet m-dimethylamino phenyloxenium ion.

Figure 3 shows a comparison between the calculated EPR spectrum of the m-dimethylamino phenyloxenium ion and the EPR obtained by the photolysis of compound **1**. There is a very strong matching of experimental and computational results, which provides further evidence for the observed triplet oxenium ion state. These signals are expected to be centered on the oxygen and nitrogen atom.

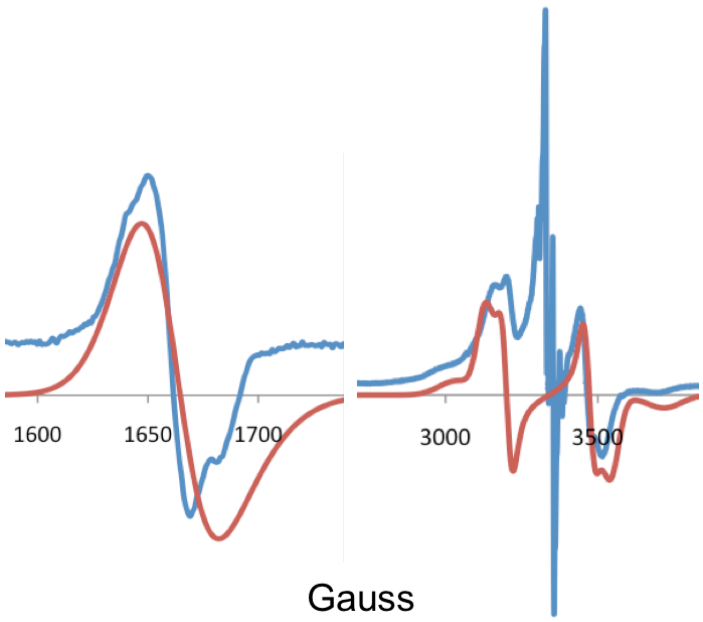

Figure 3. EPR of photolysis of compound **1** (green) compared to the computed EPR of the m-dimethylamino phenyloxenium ion**.**

The LFP studies have not yet been performed. However, basic calculations for the singlet and triplet states for the m-dimethylaminophenyloxenium ion are shown in Figure 4. This allows for some expectation of what will be observed during LFP experiments.

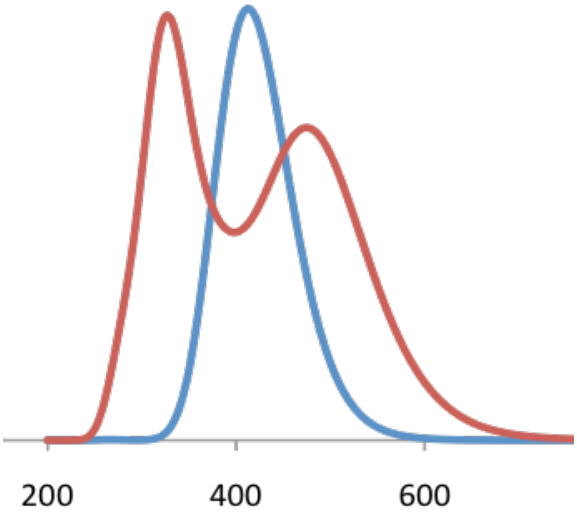

Figure 4: Computed UV-vis spectra of the singlet (blue) and triplet (red) m-dimethylamino phenyloxenium ion.

CONCLUSIONS

There is strong evidence that photolysis and thermolysis of precursor **1** lead to an oxenium ion intermediate in solution, and the triplet ground state m-dimethylamino phenyloxenium ion is indicated due to the matrix isolated EPR spectrum and B3LYP/cc-pVTZ calculations. With successful laser flash photolysis experiments we expect to provide the first direct observation of a ground state triplet oxenium ion.

Thermolytic and Photolytic conditions.

Thermolysis studies were performed by placing 10 mg of **1** in 5ml of solvent. This was then degassed and refluxed for 10 minutes. At this point starting material was completely reacted based off of ^{1}H NMR and LCMS, LCMS and ^{1}H NMR were used to evaluate products.

Photolysis studies were performed in a similar fashion. The final and deciding product studies were performed on 6 mg of **1** were placed in 3 ml of solvent. Every 5 minutes a small sample was removed and saved for LCMS analysis along with ^{1}H NMR. This was done for up to 20 minutes showing consistent product conversion. The trace products were only observed slightly by LCMS. A dimer was also observed. It is believed that as products were building up, some of the products were photosensitive. This lead to a second photoproduct to form as the dimer and the phenol, which upon complete reaction was the only product.

Synthesis of meta dimethylamino phenylhydroxylamine hydrochloride salt.

Compound **1** was made by a modified known procedure.[5]

Synthesis of *N*-m-dimethylaminophenoxyphthalimide. 326 mg (2mmol, 1eq) of N-hydroxyphthalimide, 200 mg (2mmol, 1equiv) of CuCl, 660 mg (4 mmol, 2 equiv) of phenylboronic acid, and ~500 mg of 4Å molecular sieves were added to a round bottom flask. 15 mL of 1,2-dichloroethane followed by 180 μL (2.2 mmol, 1.1 equiv) of pyridine were added to the flask. The reaction was stirred for 72 hours under air at ambient temperature. The reaction was monitored by TLC (75:25 Hexanes:Ethyl Acetate). The reaction was allowed to react for 72 h and then the solvent was evaporated under reduced pressure. The product was separated by column chromatography (7:3 Hexanes:Ethyl Acetate). A white solid (N-meta dimethylaminophenylphthalimide) was collected and dried by high vacuum, to give 60% yield (277.6 mg), of the desired product. This product was then used for the next step in the synthesis.

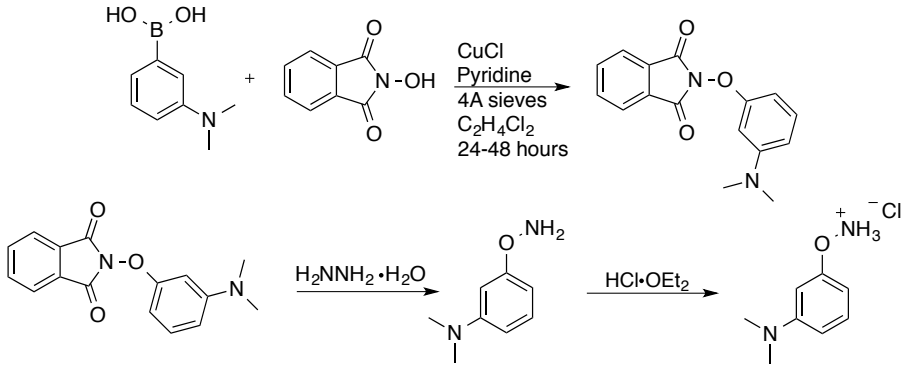

Figure 5: Synthetic route for the formation of product **1.**

^{1}H NMR for intermediate N-m-dimethylaminophenoxypthalimide

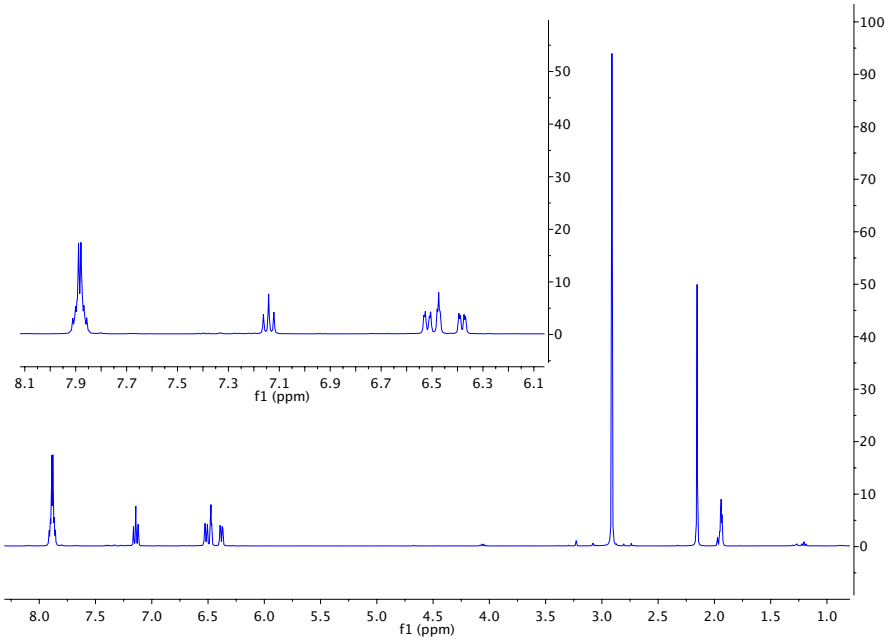

Synthesis of m-dimethylaminophenylhydroxylamine hydrochloride 1. 277.6 mg (0.98 mmol, 1 equiv) of N-phenoxyphthalamide was added to a flask containing 100 mL of 10% MeOH in $CHCl_3$ and 0.48 mL (9.8 mmol, 10 equiv) of hydrazine monohydrate. A colorless solution was formed, which yielded a white precipitate over time. The reaction was monitored by TLC (75:25 Hexanes:Ethyl Acetate) and allowed to react overnight (12 h). The filtered solid was then purified by column chromatography

(75:25 Hexanes:Ethyl Acetate). The resulting product was dissolved in ether, to which HCl*OEt_2 (ca. 0.3 mL) was added until the TLC spot no longer moved. This signified the protonation of the hydroxylamine to the hydroxylamine hydrochloride salt. This solution was then dried under reduced pressure to yield 162 mg of the desired salt. (162 mg, 87.3% yield). The product was reasonably stable stored in a freezer in the dark.

^{1}HNMR for meta dimethylamino phenylhydroxylamine hydrochloride

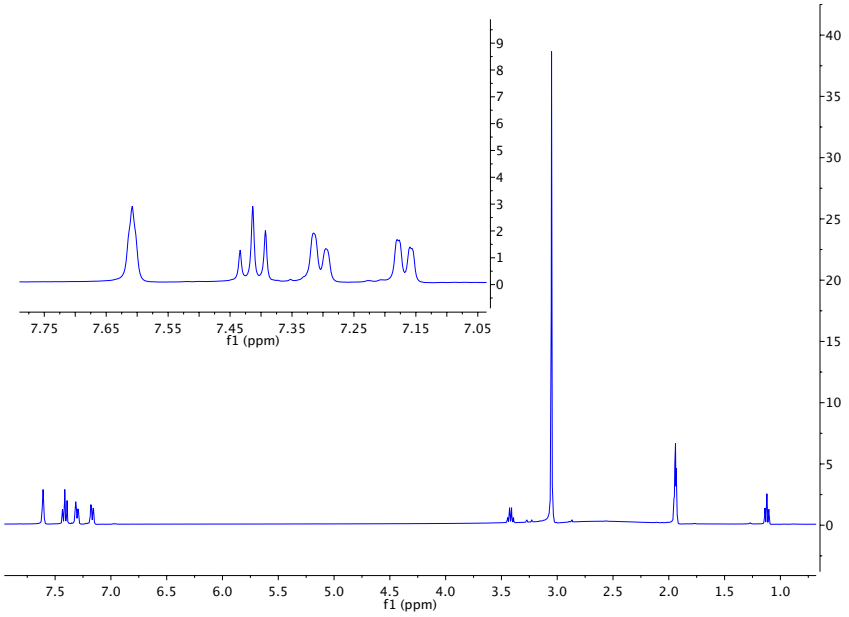

REFERENCES

(1) Hanway, P. J.; Xue, J.; Bhattacharjee, U.; Milot, M. J.; Ruixue, Z.; Phillips, D. L.; Winter, A. H. *J. Am. Chem. Soc.* **2013**, *135*, 9078.

(2) Wang, Y. T.; Wang, J.; Platz, M. S.; Novak, M. *J. Am. Chem. Soc.* **2007**, *129*, 14566.

(3) Hanway, P. J.; Winter, A. H. *J. Am. Chem. Soc.* **2011**, *133*, 5086.

(4) Frisch, M. J.; et al. *Gaussian 09,* version A02; Gaussian, Inc.: Pittsburg, PA, 2009.

(5) Petrassi, H. M.; Sharpless, K. B.; Kelly, J. W. *Organic Letters* **2000**, *3*, 139.

CONCLUSIONS

In conclusion, much has been gained in the understanding of oxenium ions. We have discovered a precursor based on protonated hydroxylamines that can generate oxenium ions via photolysis or thermolysis in a variety of solvents. We have also found computationally that oxenium ions can have ground state singlet or triplet configurations depending on the nature of the substituents. In particular, phenyloxenium ions with meta pi donors and heteroaryl oxenium ions are computed to have possible triplet ground states. Through laser flash photolysis studies and computation studies, we now have insight into oxenium ions that were previously unreported, including direct detection by LFP of closed shell singlet, open shell singlet, and triplet oxenium ions. We have also formed what we predict to be a ground state triplet oxenium ion through matrix isolated EPR studies.